Electronic Supplementary Information

Framework flexibility-driven CO_2 adsorption on a zeolite

Hyun June Choi,[a] Jung Gi Min,[a] Sang Hyun Ahn,[a] Jiho Shin,[a] Suk Bong Hong,*[a] Sambhu Radhakrishnan,[b] C. Vinod Chandran,[b] Robert G. Bell,[c] Eric Breynaert[b] and Christine E. A. Kirschhock[b]

[a] Center for Ordered Nanoporous Materials Synthesis, Division of Environmental Science and Engineering, POSTECH, Pohang 37673, Korea

[b] Center for Surface Chemistry and Catalysis, Characterisation and Application Team (COK-kat), Celestijnenlaan 200 F – box 2461, KU Leuven, 3001 Heverlee, Belgium.

[c] Department of Chemistry, University College London, 20 Gordon Street, London WC1H 0AJ, UK.

*e-mail: sbhong@postech.ac.kr

Table of Contents

Section S0. Structure description of GIS-3.0

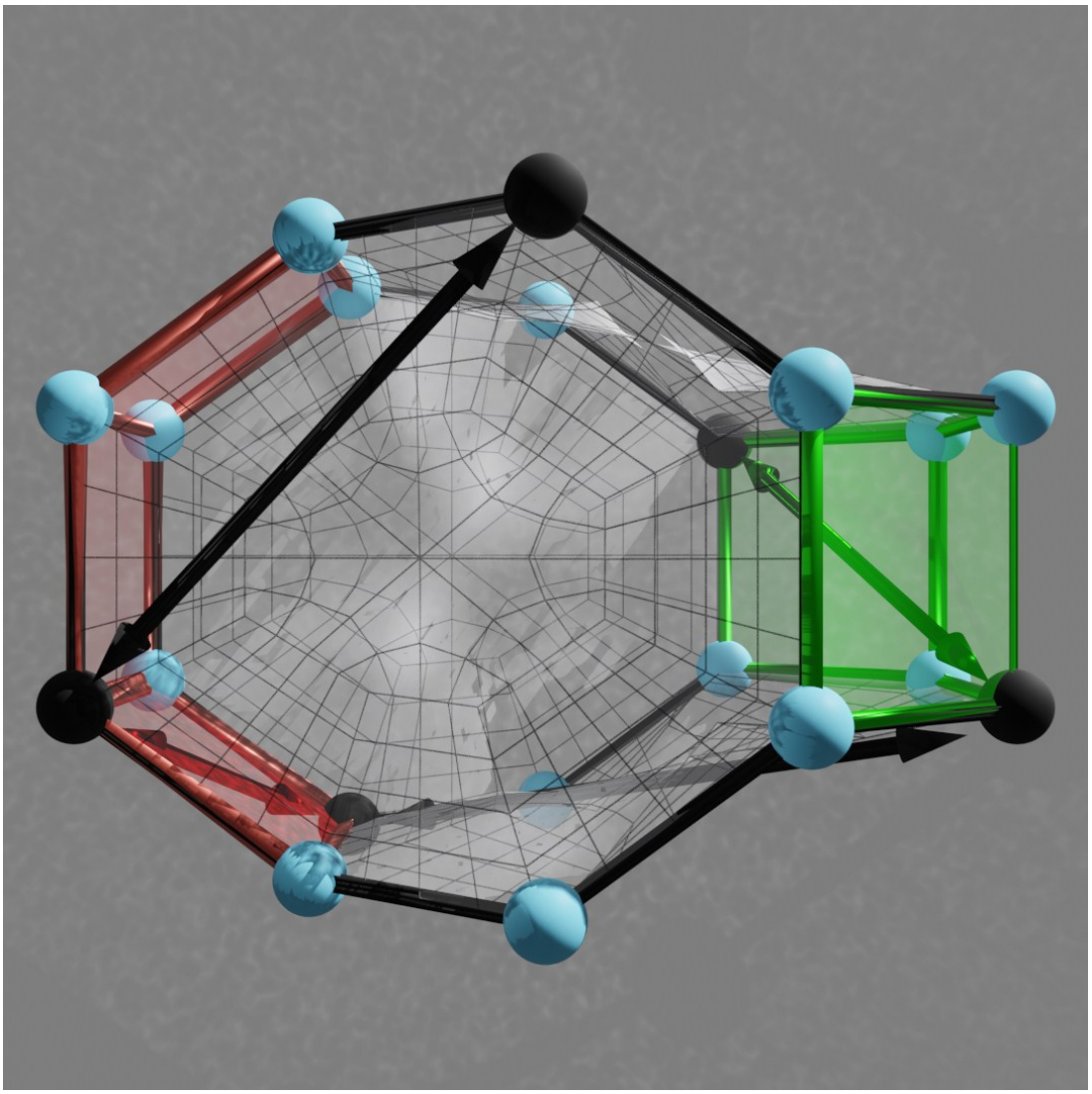

Movie 1: Click to play. The GIS topology can be entirely constructed by laterally connecting 4 double-crankshaft chains (*dcc*s), which are related by unit translations and glide-mirror operations (green *dcc*). This creates the *gis*-cage (*t-gsm*, gray wireframe) and at the same time generates a second set of *dcc* (in red), related to the green set by a 4_1 symmetry operation. The GIS topology shows a pseudo-cubic symmetry in space group $P4_1/amd$. In GIS-3.0 powder X-ray diffraction and solid-state nuclear magnetic resonance (NMR) analyses revealed a significantly lower symmetry, owing to the preferential Al occupation of one of the four crystallographic sites in $P2_1/n$ (Al is shown as black, Si as light blue spheres). The *dcc*s run along the monoclinic *b* (green *dcc*) and *a* (red *dcc*) axes, which are no longer crystallographically equivalent. Four-membered rings (4-MRs) along *b* contain exactly one Al each, on alternating sides of the *dcc* (green arrows). Along *a*, every fourth 4-MR contains two Al atoms on opposite corners (red arrow). This results in the presence of two types of pockets and two types of 8-MRs. The red pocket contains an Al-pair on one side and no Al on the other, while the green pocket contains one Al on both sides across from each other. The 8-MRs delineating the channel along the *a* axis show Al exactly opposing each other, while in the 8-MR channels along the *b* axis they are separated by two Si atoms on one side and four Si atoms on the other side (black arrows).

Section S1 Synthesis of GIS-3.0 and GIS-4.7.

S1.1 Organic structure-directing agent (OSDA) synthesis

In a typical synthesis of 2-amino-*N,N,N*-trimethylethanaminium chloride (ATMEACl), the OSDA used in the synthesis of GIS-4.7 (the number in sample identification indicates the framework Si/Al ratio determined by elemental analysis), 17.63 g of *N,N*-dimethylethylenediamine (98%, TCI) was dissolved in 100 mL of methanol (99.9%, Samchun) and cooled in an ice-bath. After slowly adding 48.1 g of di-*tert*-butyl pyrocarbonate (97%, Alfa Aesar) to this solution, the mixture was allowed to slowly warm to room temperature and stirred for 1 day. The methanol in the mixture was removed using a rotary evaporator at 70 °C, and the solid product obtained was dissolved in 100 mL of water and extracted three times with 20 mL of dichloromethane (99.9%, Samchun). After drying the dichloromethane extract using sodium sulfate (99%, Samchun), the mixture was filtered and dichloromethane was removed using a rotary evaporator at 60 °C. Then, the resulting product was dissolved in 100 ml of acetonitrile (99.5%, Samchun) and cooled in an ice-bath. To this solution, 56.8 g of methyl iodide (99.5%, TCI) was slowly added, warmed to room temperature and stirred for 1 day. After removing the solvent and excess methyl iodide using rotary evaporation at 80 °C, the solid product was dissolved in 100 mL of methanolic HCl (3.0 N, Aldrich) and stirred for 2 days. Finally, the resulting precipitate was filtered and recrystallized from ether (99% Samchun), giving ATMEACl.

S1.2 Zeolite synthesis

Na-GIS-1.5 and Na-GIS-3.0 were synthesized using two aluminosilicate gels of molar compositions $10.0Na_2O•1.0Al_2O_3•10.0SiO_2•220H_2O$ and $2.5Na_2O•1.0Al_2O_3•10.0SiO_2•220H_2O$, respectively (Table S1). These synthesis gels were prepared by combining NaOH (50% aqueous solution, Aldrich), Al powder (99.5%, Wako), colloidal silica (Ludox HS-40, Aldrich), and deionized water. Further details of Na-GIS-3.0 synthesis are given in Table S1. GIS-4.7 was synthesized using an aluminosilicate gel of the molar composition $4.5ATMEACl•9.0Na_2O•1.0Al_2O_3•30.0SiO_2•1200H_2O$, where ATMEACl was prepared following the procedure described above, and NaOH (50% aqueous solution, Aldrich), $Al(NO_3)_3•9H_2O$ (98%, Junsei), and fumed silica (Aerosil 200, Degussa) were used as Na, Al, and Si sources, respectively. The final synthesis mixture was stirred at room temperature for 1 day, charged into Teflon-lined 23-mL autoclaves and heated at 150 °C under rotation (60 rpm) for 3-7 days. ^{13}C MAS NMR shows that the ATMEA ions used as an OSDA in the synthesis of GIS-4.7 are occluded intact within the crystallized product (Fig. S2). It should be noted that the gel composition ranges leading to GIS-3.0 and GIS-4.7 are both very narrow. As-synthesized GIS-4.7 was calcined at 550 °C in air for 8 h to remove the OSDA occluded and thereafter converted to its Na^+ form by refluxing four times in 1.0 M $NaNO_3$.

All zeolites synthesized here were characterized by Powder X-ray diffraction (PXRD), thermal and elemental analyses, and scanning electron microscopy (SEM) and their Na form was refluxed four times in 1.0 M aqueous nitrate solutions (1.0 g solid/ 100 mL solution) of Li^+, K^+, Rb^+, and Cs^+ ions at 80 °C for 6 h and dried at atmospheric temperature overnight. For comparison, zeolites Na-A (Si/Al = 1.0) and Na-X (Si/Al = 1.3) were obtained from Aldrich.

Table S1 Representative synthesis results[a]

Run	Gel composition		Product[b]		Solution pH[c]	Si/Al in the product[d]
	Si/Al	Si/OH	T = 100 °C	T = 150 °C		
1	5.0	0.50	Na-GIS	Na-CAN + Na-ANA	14.1	1.5
2	5.0	0.56	Na-GIS	Na-ANA	14.0	-[e]
3	5.0	0.63	Na-GIS	Na-ANA	13.9	1.7
4	5.0	0.71	Na-FAU + Na-GIS	Na-ANA	13.9	-[e]
5	5.0	0.83	Na-FAU + Na-GIS	Na-ANA	13.9	-[e]
6	5.0	1.00	Na-FAU + Na-GIS	Na-ANA	13.8	-[e]
7	5.0	1.25	Na-FAU + Na-GIS	Na-ANA	13.8	-[e]
8	5.0	1.67	Unknown	Na-GIS + Na-ANA	13.7	-[e]
9	5.0	2.00	Unknown[f]	Na-GIS	13.7	3.0
10[g]	5.0	2.00	-[h]	Na-GIS + unknown	13.7	-[e]
11	10.0	2.00	-[h]	Na-MOR	-[e]	-[e]
12	7.5	2.00	-[h]	Na-MOR	-[e]	-[e]
13	3.8	2.00	-[h]	Na-GIS + Na-ANA	-[e]	-[e]
14	2.5	2.00	-[h]	Na-GIS + Na-ANA	-[e]	-[e]
15	5.0	2.50	Amorphous[f]	Na-MOR	13.6	-[e]
16	5.0	5.00	Amorphous[f]	Amorphous[f]	13.6	-[e]

[a] The gel composition is xNa$_2$O•yAl$_2$O$_3$ •10SiO$_2$•220H$_2$O, where x and y are varied between $1.0 \leq x \leq 10.0$ and $0.5 \leq y \leq 2.0$, respectively. Crystallization was performed under rotation (60 rpm) at 100 or 150 °C for 3 days, unless otherwise stated.

[b] The phase appearing first is the major phase.

[c] The solution pH was measured prior to heating the synthesis mixture.

[d] Determined by elemental analysis.

[e] Not measured.

[f] The product obtained after 14 days of heating.

[g] Performed under static conditions.

[h] Not performed.

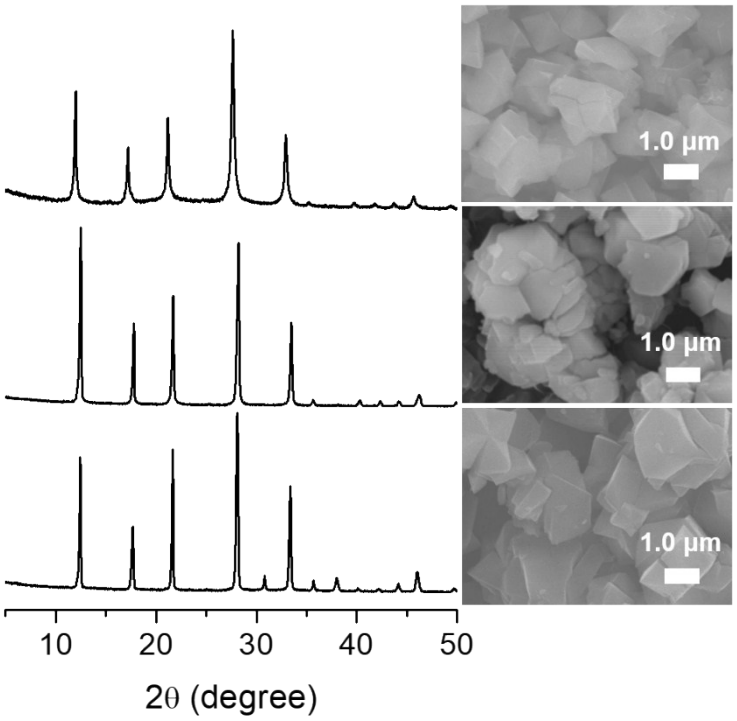

Fig. S1 PXRD patterns and SEM images of as-synthesized (from bottom to top) Na-GIS-1.5, Na-GIS-3.0, and ATMEANa-GIS-4.7. The last number in the sample identification is the zeolite Si/Al ratio determined by elemental analysis.

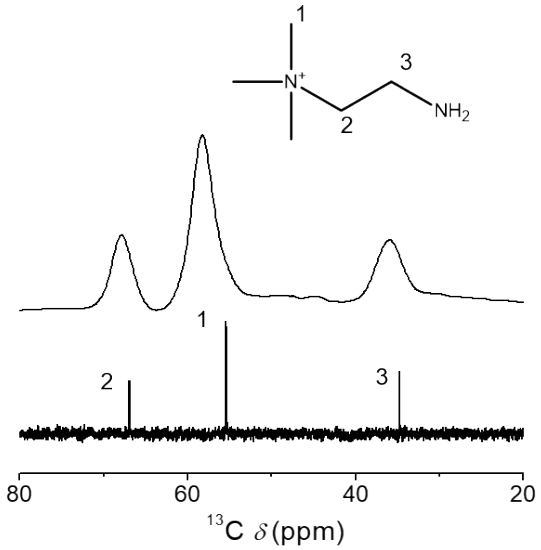

Fig. S2 ^{13}C MAS NMR spectrum of as-synthesized ATMEANa-GIS-4.7. The spectrum of 2-amino-*N,N,N*-trimethylethanaminium ions is ^{13}C NMR in D_2O solution, while that of the zeolite is ^{13}C MAS NMR of the solid.

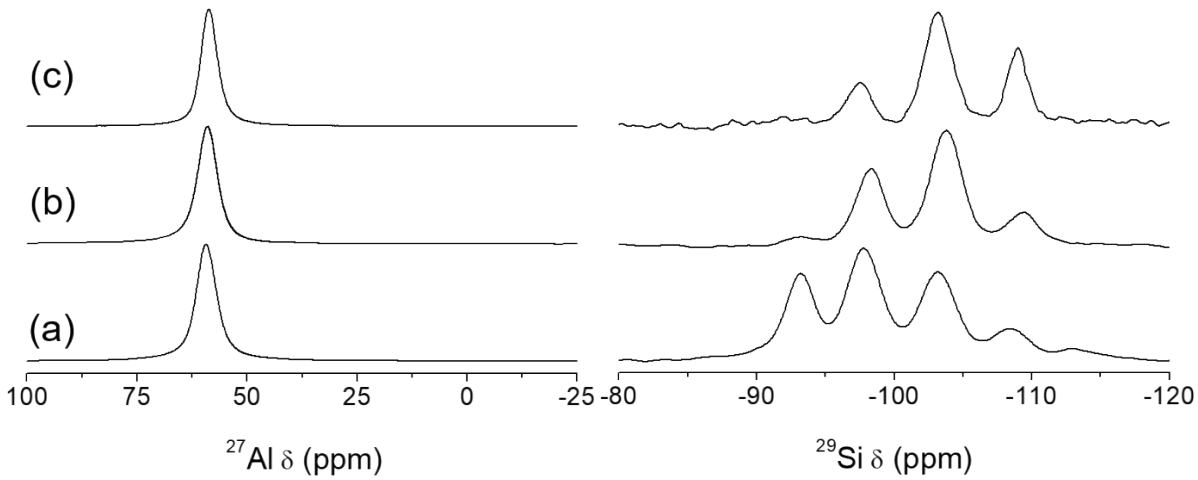

Fig. S3 ^{27}Al (left) and ^{29}Si (right) MAS NMR spectra of as-synthesized (a) Na-GIS-1.5, (b) Na-GIS-3.0, and (c) ATMEANa-GIS-4.7.

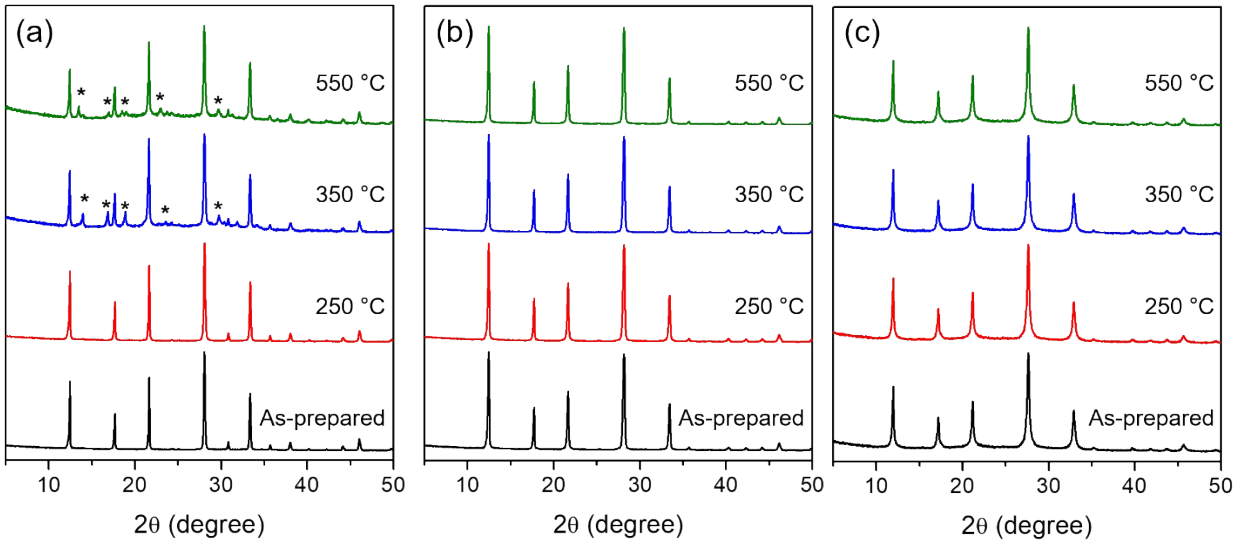

Fig. S4 PXRD patterns of (a) Na-GIS-1.5, (b) Na-GIS-3.0, and (c) Na-GIS-4.7 after heating in air at 250, 350, and 550 °C for 5 h. The X-ray reflections, which are not from the GIS structure, are marked by asterisks.

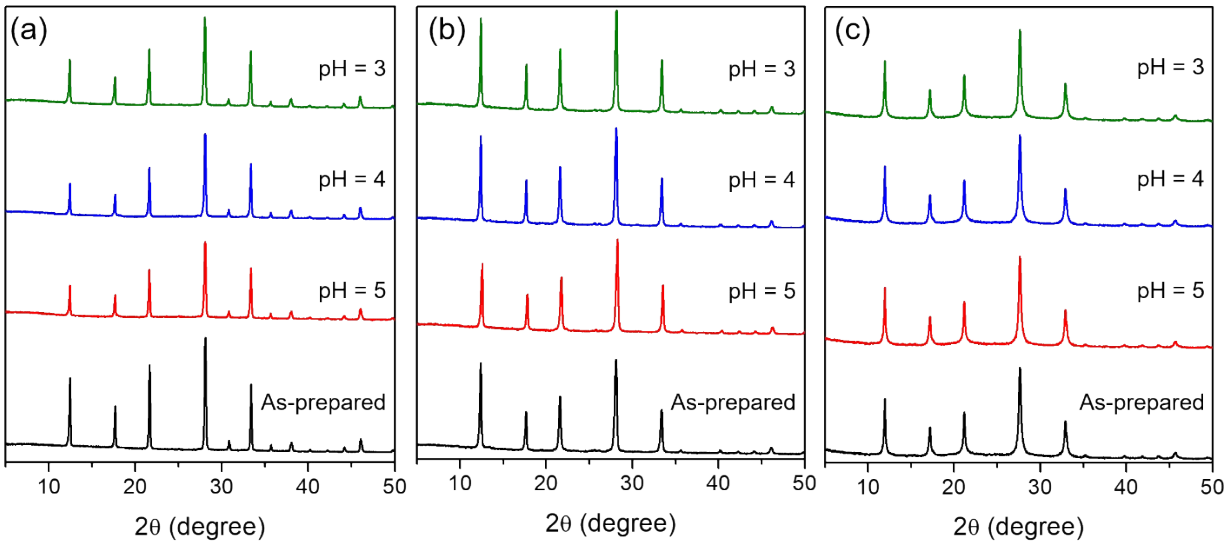

Fig. S5 PXRD patterns of (a) Na-GIS-1.5, (b) Na-GIS-3.0, and (c) Na-GIS-4.7 after stirring in aqueous 0.00001 - 0.001 M hydrochloric acid solutions (pH = 3 - 5) at 25 °C for 24 h.

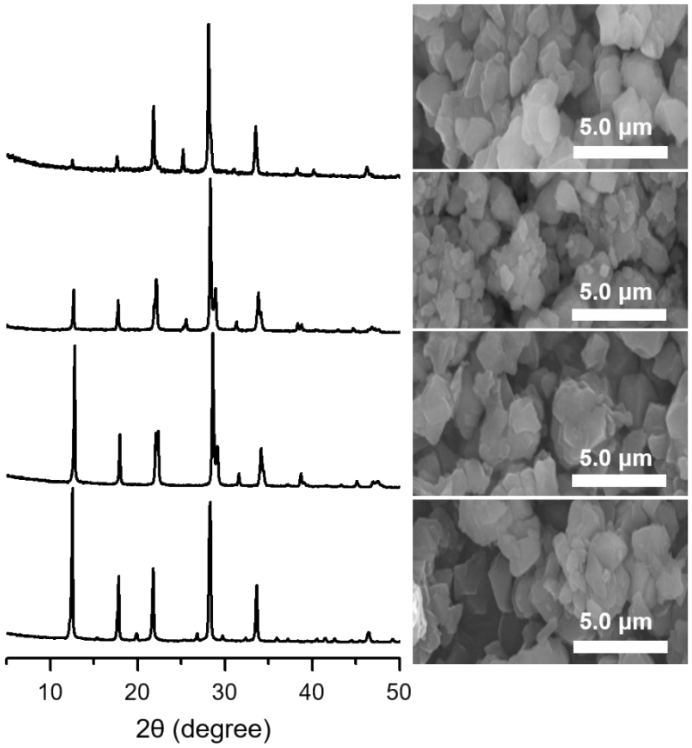

Fig. S6 PXRD patterns and SEM images of various alkali metal cation forms of GIS-3.0. From bottom to top: Li-, K-, Rb-, and Cs-GIS-3.0 zeolites.

Table S2 Chemical compositions of GIS zeolites employed in this study

Zeolite	Anhydrous unit cell composition	Degree of exchange (%)
Na-GIS-1.5	$Na_{6.4}[Al_{6.4}Si_{9.6}O_{32.0}]$	100
Li-GIS-3.0	$Li_{3.7}Na_{0.3}[Al_{4.0}Si_{12.0}O_{32.0}]$	92
Na-GIS-3.0	$Na_{4.0}[Al_{4.0}Si_{12.0}O_{32.0}]$	100
K-GIS-3.0	$K_{4.0}[Al_{4.0}Si_{12.0}O_{32.0}]$	100
Rb-GIS-3.0	$Rb_{4.0}[Al_{4.0}Si_{12.0}O_{32.0}]$	100
Cs-GIS-3.0	$Cs_{4.0}[Al_{4.0}Si_{12.0}O_{32.0}]$	100
Na-GIS-4.7	$Na_{2.8}[Al_{2.8}Si_{13.2}O_{32.0}]$	100

Section S2: Structure analysis of GIS-3.0

S2.1 Determination of the highest possible space group of Na-, K- and Rb-GIS-3.0 samples

Na-GIS-3.0 shows a Si/Al ratio of 3.0, i.e., every fourth tetrahedral site (T-site, where T is Si or Al) in the GIS topology is occupied by an Al atom. To determine whether the Al atoms are distributed randomly over the material, the one-dimensional (1D) MAS ^{29}Si NMR spectra of fully hydrated Na-, K-, and Rb-GIS-3.0 samples were analyzed in detail (Fig. S7 and Table S3). The ^{29}Si chemical shift in aluminosilicate zeolites depends on its environment and distinguishes between numbers of connected TO_4 tetrahedra and how many of those are occupied by Al. The corresponding Si atoms are known as $Q_4(n)$ Si species, where the subscript indicates the tetrahedral connections and n specifies the number of neighboring Al. All the 1D ^{29}Si MAS NMR spectra show well-resolved signals, of exclusively four-connected SiO_4 tetrahedra, wherein Si is linked to different numbers of Al, from 0 up to 3Al neighbors (Q_4(0-3)). The ^{29}Si resonances corresponding to four neighboring Al (Q_4(4)) were not observed.

To determine whether Al ordering might occur in the sample, the experimental Si distribution was compared to the expected Si distribution of the GIS topology with random Al siting. For this, a computer script was developed to generate random Al distributions, with Al occupying 25% of the T-sites in a zeolite crystal with selectable dimensions along the crystallographic axes. Generation of the Al distribution accounted for the Löwenstein rule, forbidding Al occupation of directly connected tetrahedra, and boundary Si-sites were omitted from the count. A block of 5×5×5 unit cells with GIS-connectivity was identified as sufficiently large to give reproducible $Q_4(n)$ ratios, and the simulation was repeated until the standard deviation decreased below 1%. This analysis clearly demonstrated that the Al distribution in GIS-3.0 significantly deviated from a fully random case.

We next analyzed the ^{27}Al 1D MAS NMR spectra (Fig. S6). While the ^{27}Al is of quadrupolar nature and affected by electric field gradients (EFG), in fully hydrated state with physisorbed, highly mobile water present in the pores, the ^{27}Al signal can be expected to be dominated by the framework connectivity and therefore sheds light on the number of crystallographically different Al sites. All fully hydrated samples examined show exclusively one single, Al-resonance in

tetrahedral co-ordination. The isotropic chemical shift (δ_{iso}) exhibited a downfield shift with changing extra-framework cation type in GIS-3.0 from Na^+ to K^+ to Rb^+ (Fig. S8). ^{27}Al 3Q-MAS NMR experiments revealed the presence of Al in one crystallographically distinct T-site in Na-GIS-3.0 (Fig. S8). We also examined the distribution of extra-framework cations (Na^+ and Rb^+) in hydrated Na- and Rb-GIS-3.0 samples. While ^{23}Na MAS NMR shows the presence of two distinct types of Na^+ sites in Na-GIS-3.0, ^{87}Rb MAS NMR exhibits the presence of one Rb^+ site in Rb-GIS-3.0 (Fig. S9).

With these conclusions in mind, we analyzed the synchrotron PXRD data of Na-, K- and Rb-GIS-3.0 in their hydrated, dehydrated and CO_2-loaded state (Fig. S14 and Tables S4-S13). All samples are based on exactly the same framework, which did not change or degenerate upon cation exchange or dehydration and CO_2 adsorption, as verified by solid-state NMR of cycled samples. Therefore, all samples must have a common space group, which correctly describes the favored Al distribution. It should be noted here that the truly observed symmetry of the materials could have been lowered by sample treatment, owing to site-splitting or superstructure expression. But in this case the observed space group must be a subgroup of the common highest possible symmetry imposed by Al-ordering.

Nominally, the GIS topology follows space group $I4_1/amd$, with one T-site and two oxygen sites only. Hydrated Na-GIS-3.0 could be indexed in this space group. However, hydrated K-GIS-3.0 and Rb-GIS-3.0 could only be satisfactorily indexed in *Imma*, also showing one T-site, but four oxygen sites and with symmetrically different directions along the perpendicular sets of 8-MR channels. However, neither space group can account for the Al ordering indicated by solid-state NMR. Next, the PXRD patterns of dehydrated and CO_2 loaded samples were scrutinized. All patterns consistently showed as common space group $P2_1/n$. This non-standard setting of $P2_1/c$, uses the same crystallographic directions as the description of the GIS-framework in $I4_1/amd$, which facilitates comparison of the structure changes. $P2_1/n$ requires four T-atoms with 100% occupation of sites to express the GIS connectivity. Occupation of one of these sites therefore is in perfect agreement with the observed Si/Al ratio close to 3. The resulting Al distribution is illustrated in Movie S1. This space group was then assumed to describe the framework connectivity of all samples. Testing its compliance with all experimental PXRD patterns revealed

that all of them could be satisfactorily described in this symmetry, which is in accordance with solid-state NMR.

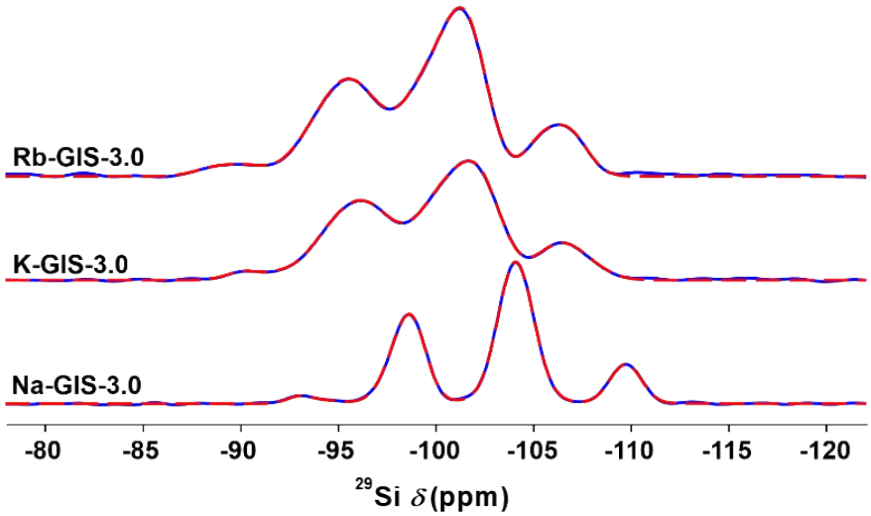

Fig. S7 1D ^{29}Si MAS NMR spectra of hydrated Na-GIS-3.0 (bottom), K-GIS-3.0 (middle) and Rb-GIS-3.0 (top): blue, experimental; red, simulated.

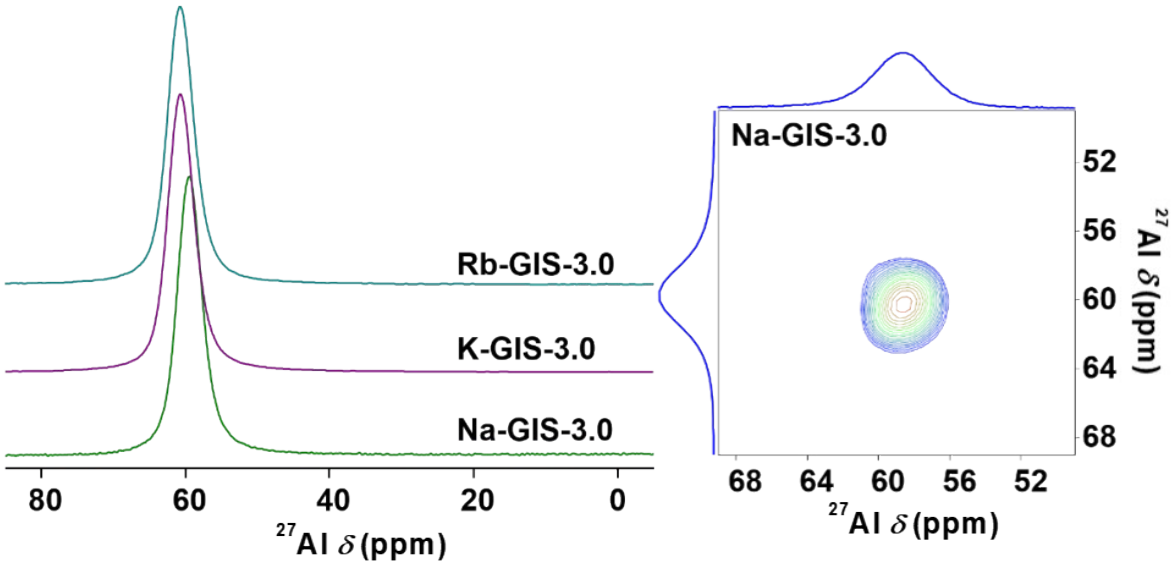

Fig. S8 ^{27}Al MAS NMR spectra (left) of hydrated Na-GIS-3.0, K-GIS-3.0 and Rb-GIS-3.0 zeolites and ^{27}Al 3Q-MAS spectrum (right) of hydrated Na-GIS-3.0

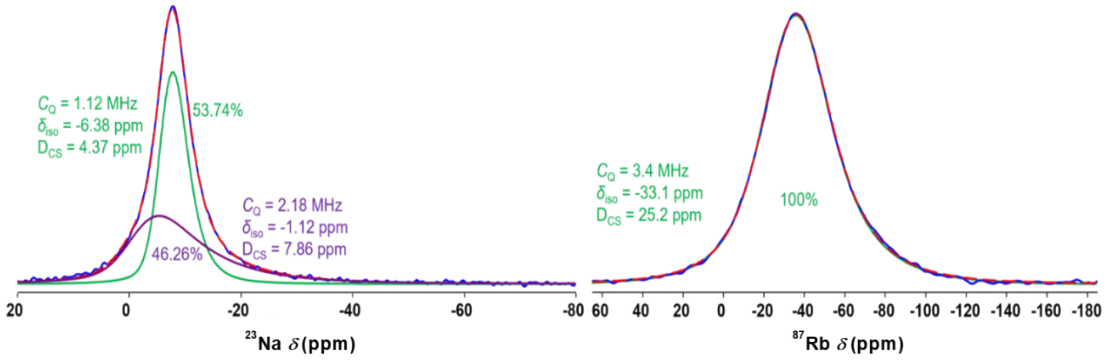

Fig. S9 ^{23}Na (left) and ^{87}Rb (right) MAS NMR spectra of hydrated Na-GIS-3.0 and Rb-GIS-3.0, respectively: blue, experimental; red, simulated; green and purple, decomposed components.

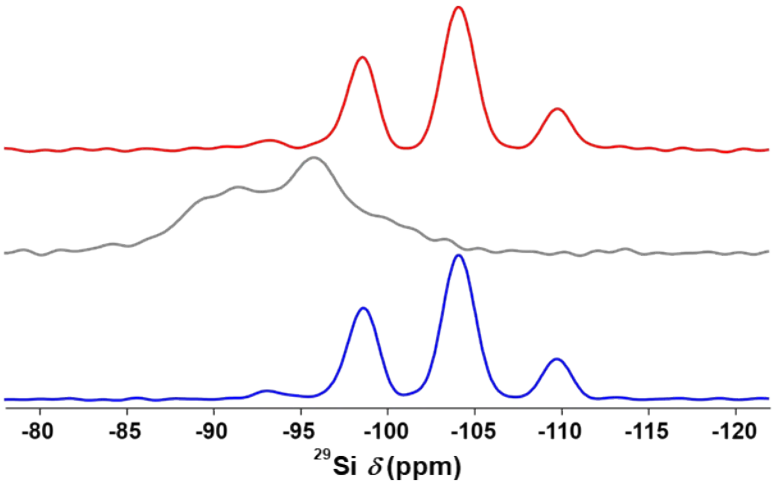

Fig. S10 1D ^{29}Si MAS NMR spectra of Na-GIS-3.0: hydrated (bottom), dehydrated (middle) and rehydrated (top) states.

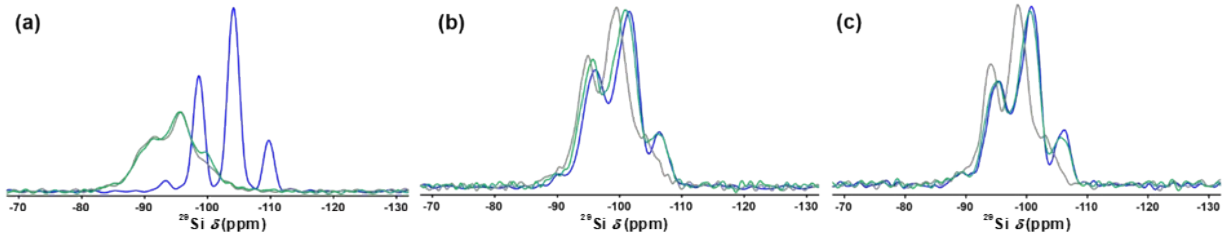

Fig. S11 ^{1}H decoupled ^{29}Si MAS NMR spectra of (a) Na-, (b) K- and (c) Rb-GIS-3.0: hydrated (blue), dehydrated (grey), and CO_2 adsorbed states (green).

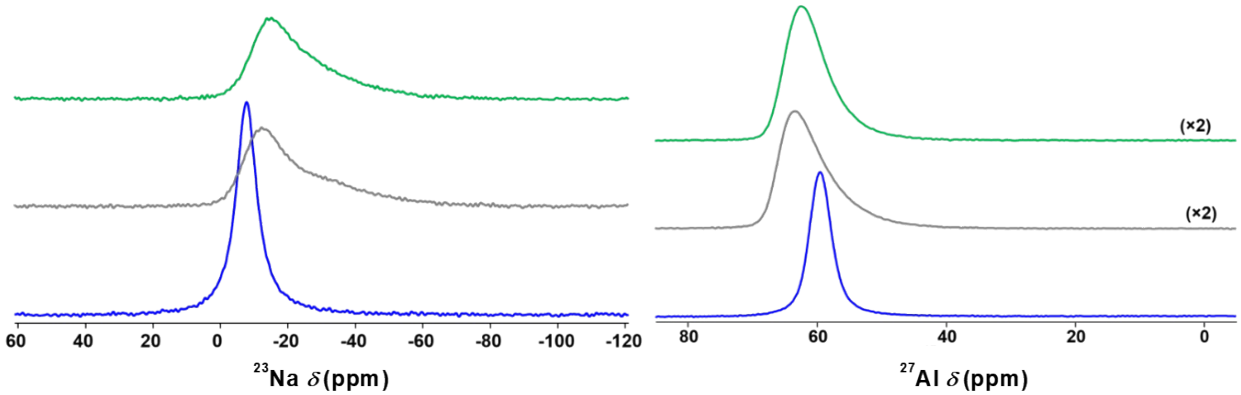

Fig. S12 Comparison of ^{23}Na (left) and ^{27}Al (right) MAS NMR spectra of Na-GIS-3.0: hydrated (blue), dehydrated (grey) and CO_2-loaded (green) states.

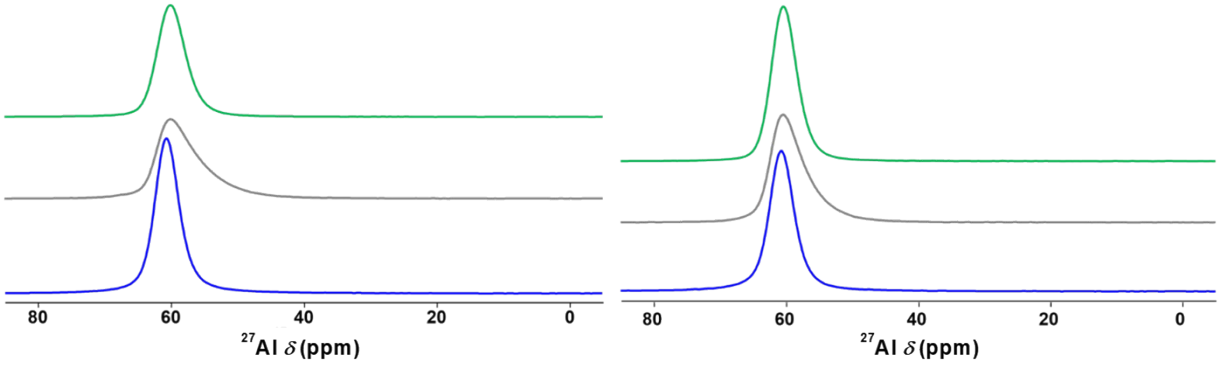

Fig. S13 Comparison of ^{27}Al MAS NMR spectra of K-GIS-3.0 (left) and Rb-GIS-3.0 (right): hydrated (blue), dehydrated (grey) and CO_2-loaded (green) states.

Table S3 Decomposition results of 1D ^{29}Si MAS NMR spectra of hydrated Na-GIS-3.0, K-GIS-3.0, and Rb-GIS-3.0

	$Q_4(0)$	$Q_4(1)$	$Q_4(2)$	$Q_4(3)$	$Q_4(4)$
Random	0.208	0.417	0.307	0.100	0.016
Std dev.	0.009	0.009	0.010	0.008	0.004
Na-GIS-3.0	0.122	0.536	0.314	0.028	0
K-GIS-3.0	0.123	0.492	0.362	0.024	0
Rb-GIS-3.0	0.128	0.523	0.316	0.033	0

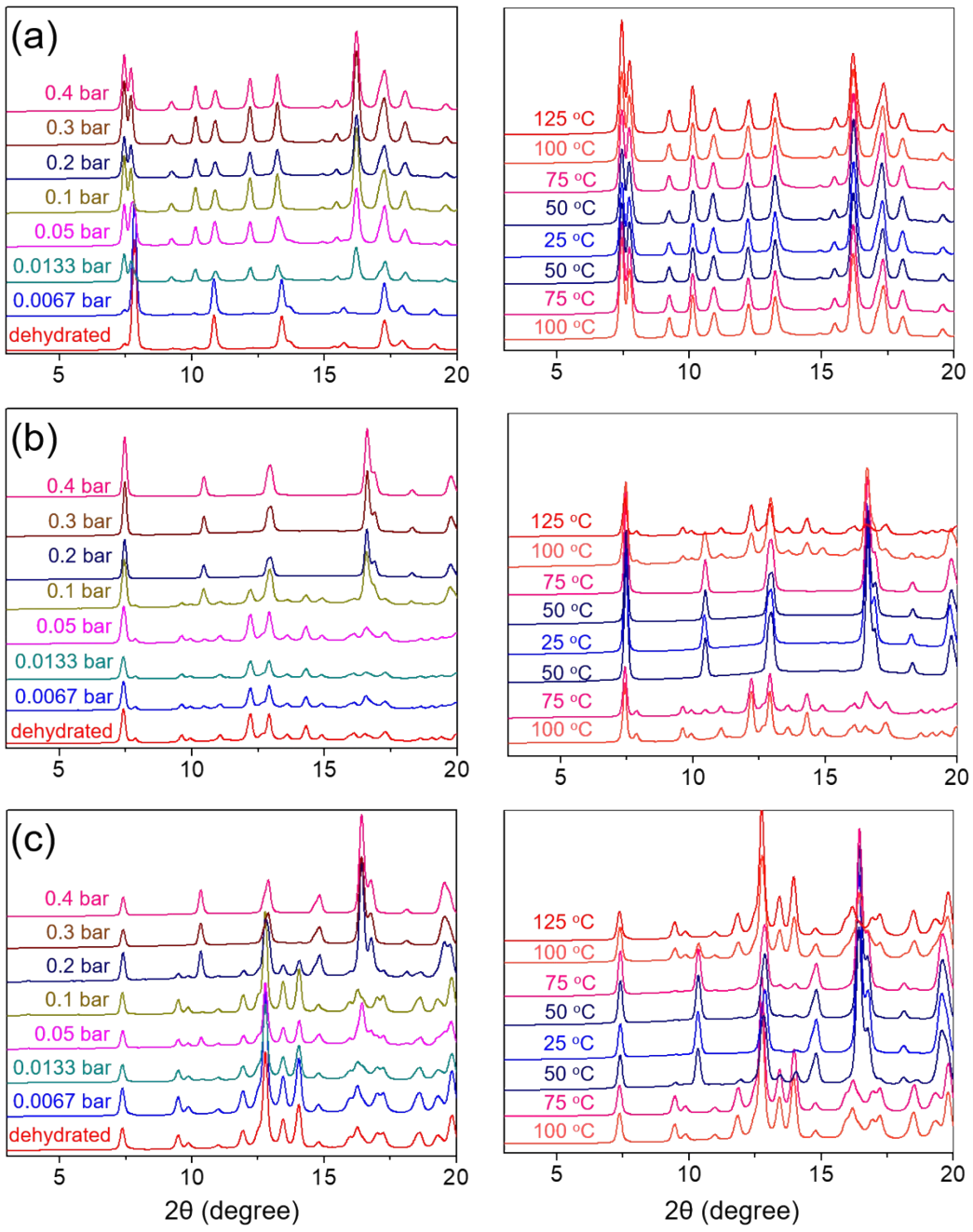

Fig. S14 Synchrotron PXRD patterns of (a) Na-GIS-3.0, (b) K-GIS-3.0, and (c) Rb-GIS-3.0 at 25 °C and different CO_2 pressures (left panels) and at different temperatures in 1.0 bar CO_2 (right panels). All patterns were measured using monochromated X-rays (λ = 0.9000 Å).

S2.2 Refinement of GIS-3.0 samples

As outlined above, all PXRD patterns could successfully be indexed in space group $P2_1/n$. However, the close similarity of the lattice parameters required a closer analysis to determine the crystallographic orientation of the GIS topology. This was achieved using the program FOX.[S1] The GIS structure was introduced as its asymmetric unit, a single 4-MR, containing one Al and three Si sites and the corresponding oxygen sites. Monte-Carlo modelling, allowing also for optimisation of the zeolite fragment quickly revealed the accurate assignment of crystallographic direction to be used in Rietveld refinement. Next, the zeolite topology was optimized in GULP[S2,S3] using the Catlow library.[S4,S5] In the case of Na^+, an attempt was also made to obtain starting positions by force-field modelling in GULP, similar as for CO_2, using force-field parameters adapted from work of Bell and co-workers[S6]. For K-GIS-3.0 and Rb-GIS-3.0, cation positions were readily revealed by inspecting the difference electron density maps. PXRD data were refined using the GSAS program suite[S7,S8]. Absorption corrections were introduced according to the chemical composition. As starting coordinates, the values obtained by Force-field optimization were used. Bond lengths and angles of the framework initially were constrained, and during proceeding refinement the weight of constraints was lowered. CO_2 molecules were introduced as rigid body and left freely to move and orient.

Table S4 Crystallographic data for hydrated, dehydrated, and CO_2-loaded GIS-3.0 samples

Sample	Hydrated Na-GIS-3.0	Dehydrated Na-GIS-3.0	CO_2-loaded Na-GIS-3.0	Hydrated K-GIS-3.0	Dehydrated K-GIS-3.0	CO_2-loaded K-GIS-3.0
Symmetry	Monoclinic	Monoclinic	Monoclinic	Monoclinic	Monoclinic	Monoclinic
Space group	$P2_1/n$	$P2_1/n$	$P2_1/n$	$P2_1/n$	$P2_1/n$	$P2_1/n$
a (Å)	9.99794 (8)	9.5740 (8)	9.4065 (5)	9.6692 (4)	8.570 (5)	9.7097 (3)
b (Å)	9.98928 (7)	10.2033 (9)	10.0774 (4)	9.8778 (3)	9.461 (5)	9.8590 (3)
c (Å)	10.05969 (8)	8.9807 (11)	9.2431 (4)	9.8596 (4)	10.517 (6)	9.8932 (2)
β (°)	90.0375 (10)	91.021 (12)	90.489 (6)	90.001 (6)	90.207 (6)	90.399 (4)
Unit cell volume (Å^3)	1004.68 (1)	877.12 (10)	876.14 (9)	941.69 (10)	852.7 (14)	947.03 (5)
Diffractometer	9B, PAL	2D, PAL	2D, PAL	9B, PAL	2D, PAL	9B, PAL
Wavelength (Å)	1.5175	0.9000	0.9000	1.5175	0.9000	1.5177
2θ scan range (°)	7.01-127.510	3.202-60.167	3.374-59.902	7.00-127.50	4.976-59.899	4.966-125.466
2θ step size (°)	0.010	0.017	0.017	0.010	0.017	0.020
Least-squares matrix	full, 98 parameters	full, 62 parameters	full, 84 parameters	full, 70 parameters	full, 90 parameters	full, 148 parameters
R_p	0.074	0.082	0.053	0.070	0.055	0.047
R_{wp}	0.101	0.102	0.067	0.078	0.091	0.064
R_{exp}	0.044	0.041	0.012	0.039	0.032	0.032
$R(F^2)$	0.0955	0.101	0.0983	0.0910	0.1060	0.12884
$(\Delta/\sigma)_{max}$	0.24	0.19	0.65	1.25	1.72	1.72

Sample	Hydrated Rb-GIS-3.0	Dehydrated Rb-GIS-3.0	CO_2-loaded Rb-GIS-3.0
Symmetry	Monoclinic	Monoclinic	Monoclinic
Space group	$P2_1/n$	$P2_1/n$	$P2_1/n$
a (Å)	9.7445 (8)	8.6476 (3)	10.0083 (2)
b (Å)	9.9703 (8)	9.3960 (3)	10.02463 (11)
c (Å)	9.9551 (8)	10.4845 (3)	9.7416 (2)
β (°)	90.009 (2)	89.994 (12)	89.997 (12)
Unit cell volume (Å^3)	967.20 ()	851.90 (3)	977.36 (3)
Diffractometer	9B, PAL	2D, PAL	2D, PAL
Wavelength (Å)	1.5175	0.6927	0.6927
2θ scan range (°)	6.991-127.491	2.042-45.042	2.022-45.022
2θ step size (°)	0.010	0.010	0.010
Least-squares matrix	full, 71 parameters	full, 66 parameters	full, 68 parameters
R_p	0.059	0.038	0.032
R_{wp}	0.079	0.056	0.052
R_{exp}	0.010	0.003	0.023
$R(F^2)$	0.1272	0.10629	0.1057
$(\Delta/\sigma)_{max}$	1.68	1.86	1.62

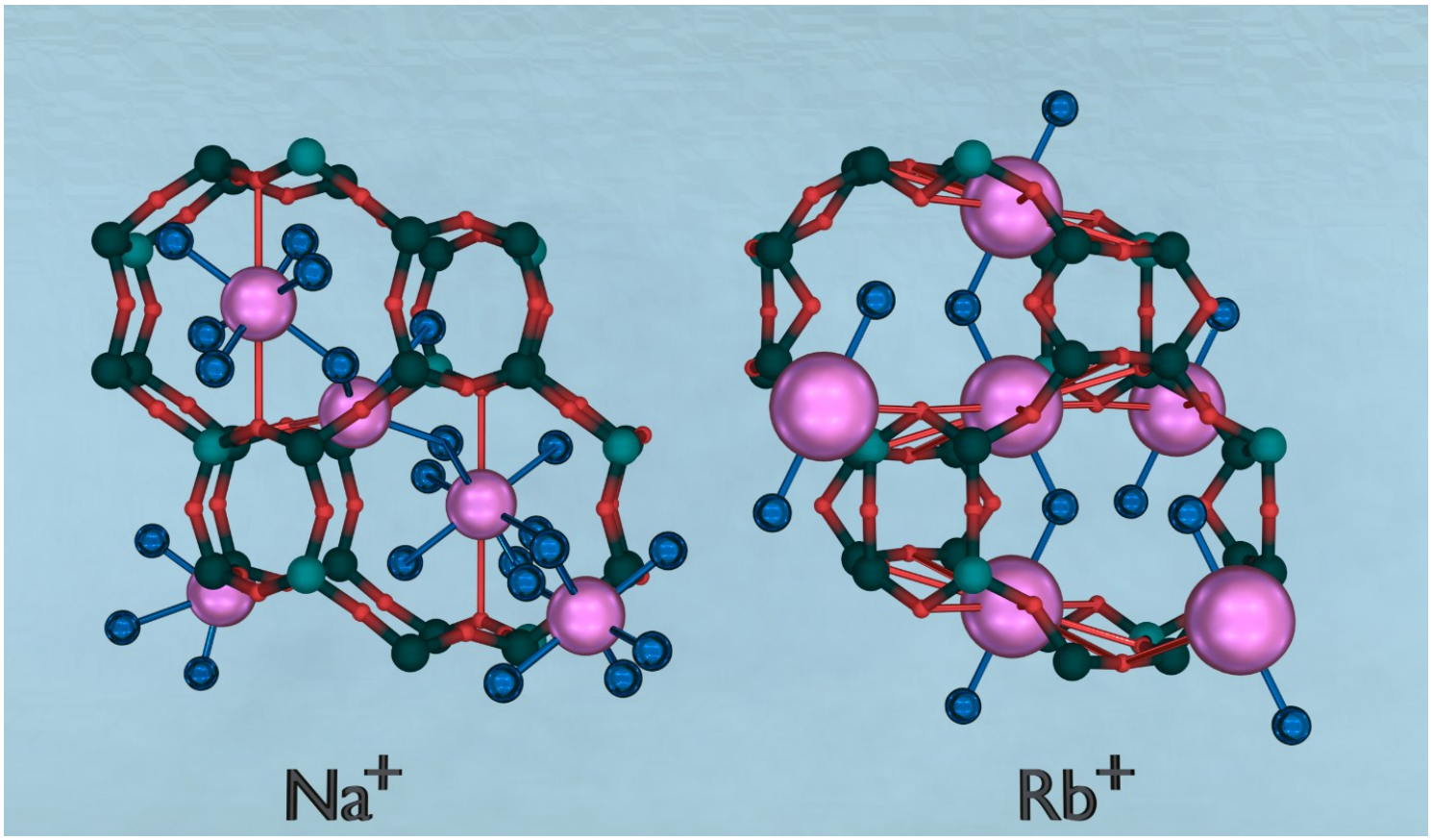

Movie 2: Structural changes of Na-GIS-3.0 (left) compared to Rb-GIS-3.0 (right); click to play

Table S5 Refined XRD-pattern and parameters of hydrated Na-GIS-3.0

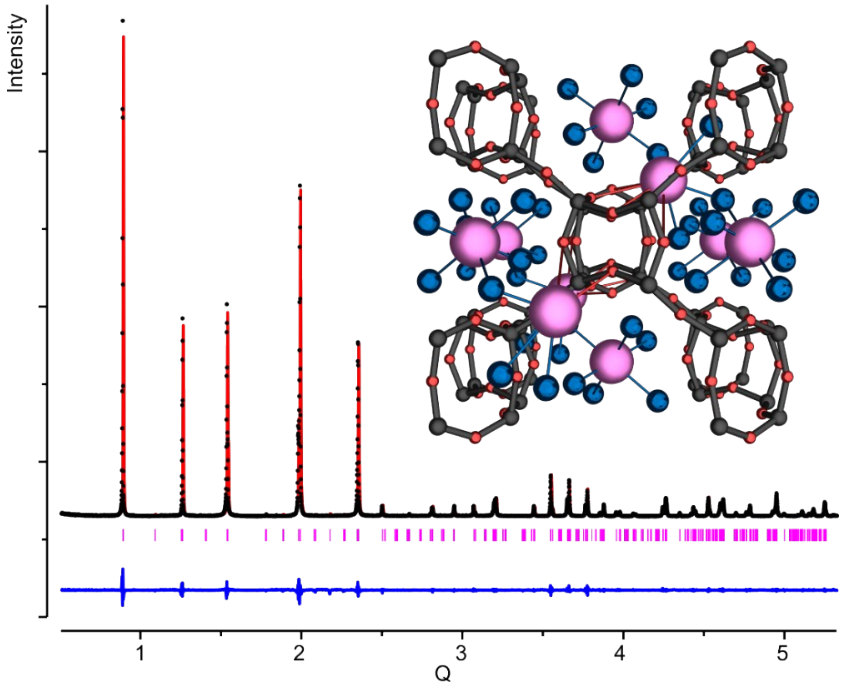

Fractional atomic coordinates and isotropic or equivalent isotropic displacement parameters (Å²)

	x	*y*	*z*	U_{iso}	Occ. (<1)
O1	0.42602 (5)	0.00100 (1)	0.18209 (4)	0.015 (2)	
O2	0.55398 (4)	0.50052 (8)	0.64642 (2)	0.027 (3)	
O3	0.25182 (9)	0.67140 (7)	0.41603 (1)	0.019 (8)	
O4	0.24820 (9)	0.82870 (7)	0.08431 (3)	0.026 (4)	
O5	0.44019 (4)	0.25783 (4)	0.24402 (4)	0.026 (4)	
O6	0.55971 (4)	0.25802 (4)	0.75618 (4)	0.018 (3)	
O7	0.00302 (3)	0.60721 (5)	0.50001 (9)	0.014 (3)	
O8	0.0000 (2)	0.78532 (2)	0.000 (2)	0.028 (7)	
Si1	0.40351 (3)	0.15124 (8)	0.12805 (8)	0.013 (6)	
Si2	0.59072 (4)	0.34298 (7)	0.62079 (9)	0.010 (4)	
Al3	0.40933 (4)	0.34326 (7)	0.37906 (9)	0.039 (2)	
Si4	0.59652 (3)	0.15089 (8)	0.87255 (8)	0.010 (4)	
Na1	0.8051 (2)	−0.2623 (2)	0.3023 (6)	0.023 (5)	0.5
Na2	0.0	0.5	0.0	0.030 (2)	
ow1	0.174 (2)	0.339 (7)	0.922 (5)	0.025 (4)	
ow2	0.897 (2)	0.353 (2)	0.185 (7)	0.031 (8)	
ow3	0.149 (2)	0.570 (5)	0.150 (4)	0.033 (2)	
ow4	0.264 (6)	0.549 (7)	0.616 (4)	0.032 (5)	0.5
ow5	0.140 (5)	−0.012 (5)	0.733 (3)	0.040 (1)	0.5

Crystal data
Monoclinic, $P2_1/n$
a = 9.99794 (8) Å
b = 9.98928 (7) Å
c = 10.05969 (8) Å
β = 90.0375 (10)°
V = 1004.68 (1) Å³

Data collection
$2\theta_{min}$ = 7.010°, $2\theta_{max}$ = 127.510°,
$2\theta_{step}$ = 0.01°
Wavelength, 1.5175 Å

Refinement
Least-squares matrix: full, 98 Parameters
R_p = 0.074
R_{wp} = 0.101
R_{exp} = 0.044
$R(F^2)$ = 0.0955
12051 data points
$(\Delta/\sigma)_{max}$ = 0.24

Table S6 Refined XRD-pattern and parameters of dehydrated Na-GIS-3.0

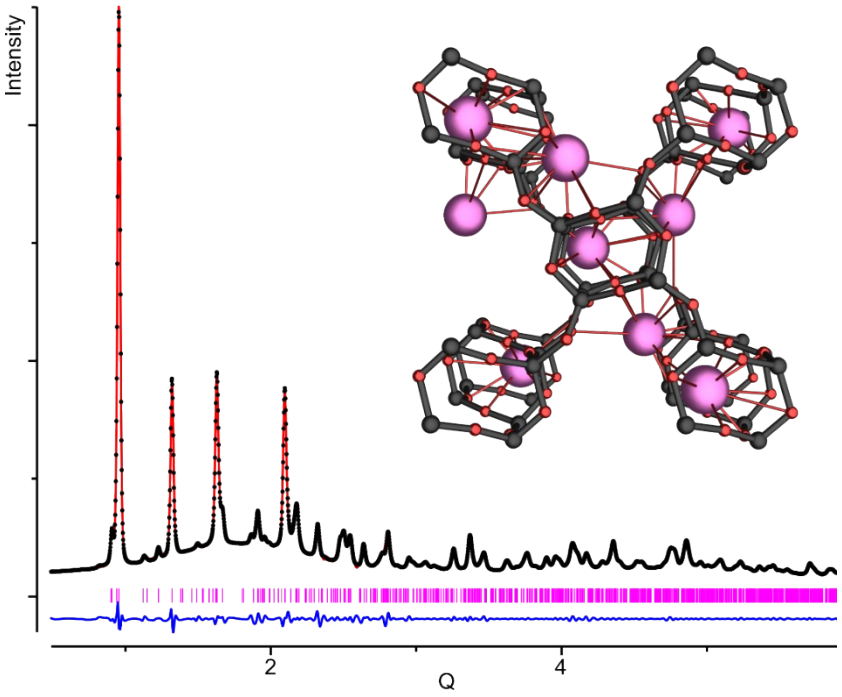

Fractional atomic coordinates and isotropic or equivalent isotropic displacement parameters ($Å^2$)

	x	*y*	*z*	U_{iso}	Occ. (<1)
Si1	0.4162 (1)	0.1722 (2)	0.1070 (1)	0.013	
Al2	0.4153 (5)	0.4080 (6)	0.3053 (2)	0.016	
Si3	0.0755 (9)	0.4040 (6)	0.3047 (6)	0.015	
Si4	0.0855 (6)	0.1751 (9)	0.1149 (4)	0.014	
O1	0.2393 (7)	0.3777 (5)	0.3334 (9)	0.020	
O2	0.2499 (9)	0.1866 (6)	0.0828 (6)	0.021	
O3	0.0237 (4)	0.3171 (4)	0.1635 (3)	0.018	
O4	0.4772 (1)	0.3083 (5)	0.1661 (4)	0.015	
O5	0.0509 (8)	0.5580 (2)	0.2714 (4)	0.012	
O6	0.5068 (3)	0.3746 (4)	0.4674 (5)	0.019	
O7	0.4886 (2)	0.1366 (2)	0.9506 (1)	0.030	
O8	0.0615 (9)	0.0709 (1)	0.2454 (2)	0.021	
Na1	0.718 (3)	0.489 (3)	0.412 (9)	0.0311	0.5
Na2	0.764 (3)	0.351 (2)	0.821 (4)	0.0321	0.5

Crystal data
Monoclinic, $P2_1/n$
a = 9.5740 (8) Å
b = 10.2033 (9) Å
c = 8.9807 (11) Å
β = 91.021 (12)°
V = 877.12 (10) Å^3

Data collection
$2\theta_{min}$ = 3.202°, $2\theta_{max}$ = 60.167°,
$2\theta_{step}$ = 0.017°
Wavelength, 0.9 Å

Refinement
Least-squares matrix: full, 62 Parameters
R_p = 0.082
R_{wp} = 0.102
R_{exp} = 0.041
$R(F^2)$ = 0.101
3443 data points
$(\Delta/\sigma)_{max}$ = 0.19

Table S7 Refined XRD-pattern and parameters of CO_2-loaded Na-GIS-3.0

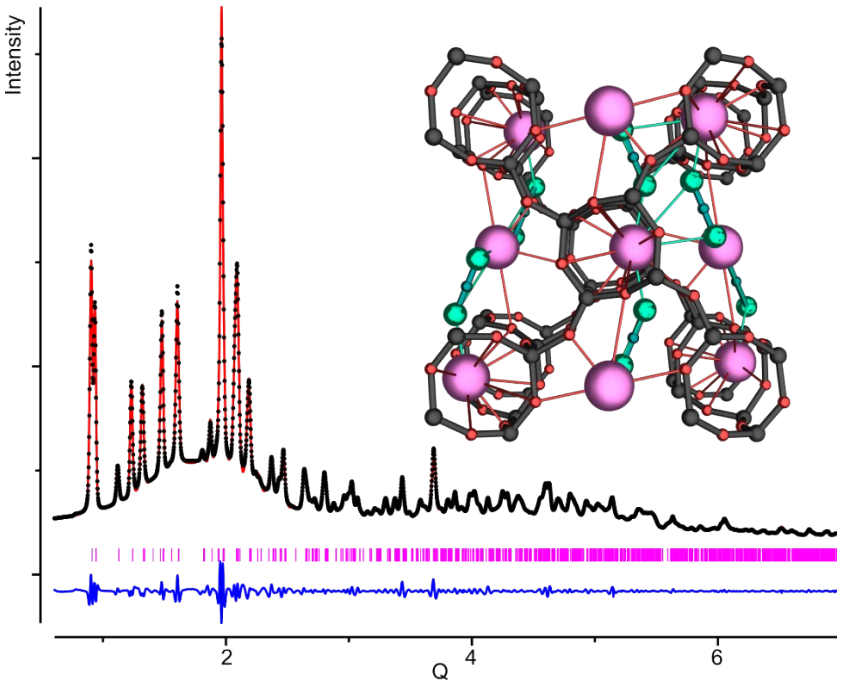

Fractional atomic coordinates and isotropic or equivalent isotropic displacement parameters ($Å^2$)

	x	*y*	*z*	U_{iso}	Occ. (<1)
Si1	0.4131 (3)	0.1851 (2)	0.0907 (4)	0.019 (8)	
Al2	0.4154 (4)	0.3991 (9)	0.3152 (6)	0.018 (3)	
Si3	0.0825 (1)	0.3996 (2)	0.3184 (3)	0.016 (6)	
Si4	0.0803 (6)	0.1868 (3)	0.0968 (5)	0.012 (2)	
O1	0.2414 (8)	0.3731 (1)	0.3542 (3)	0.017 (3)	
O2	0.2472 (4)	0.1900 (6)	0.0591 (5)	0.016 (4)	
O3	0.0362 (8)	0.3294 (6)	0.1685 (6)	0.014 (6)	
O4	0.4661 (7)	0.3168 (3)	0.1614 (7)	0.056 (7)	
O5	0.0470 (7)	0.5569 (9)	0.3076 (1)	0.011 (6)	
O6	0.5011 (2)	0.3218 (5)	0.4501 (5)	0.013 (6)	
O7	0.4831 (7)	0.1653 (8)	0.9371 (1)	0.013 (4)	
O8	0.0490 (5)	0.0662 (4)	0.2017 (8)	0.012 (4)	
Na1	0.500000	0.500000	0.000000	0.025	
Na2	0.7249 (5)	0.500000	−0.6003 (2)	0.025	0.5
Co1	0.249 (3)	0.349 (1)	0.898 (3)	0.025	0.5
Co2	0.249 (3)	0.650 (1)	0.898 (3)	0.025	0.5
Oc1	0.252 (6)	0.758 (4)	0.849 (8)	0.025	0.5
Oc2	0.245 (9)	0.543 (4)	0.946 (2)	0.025	0.5
Oc3	0.252 (6)	0.241 (5)	0.849 (8)	0.025	0.5
Oc4	0.245 (9)	0.456 (5)	0.946 (2)	0.025	0.5

Crystal data
Monoclinic, $P2_1/n$
a = 9.4065 (5) Å
b = 10.0774 (4) Å
c = 9.2431 (4) Å
β = 90.489 (6)°
V = 876.14 (9) Å^3

Data collection
$2\theta_{min}$ = 3.374°, $2\theta_{max}$ = 59.902°,
$2\theta_{step}$ = 0.017°
Wavelength, 0.9 Å

Refinement
Least-squares matrix: full, 84 Parameters
R_p = 0.053
R_{wp} = 0.067
R_{exp} = 0.012
$R(F^2)$ = 0.0983
3417 data points
$(\Delta/\sigma)_{max}$ = 0.65

Table S8 Refined XRD-pattern and parameters of hydrated K-GIS-3.0

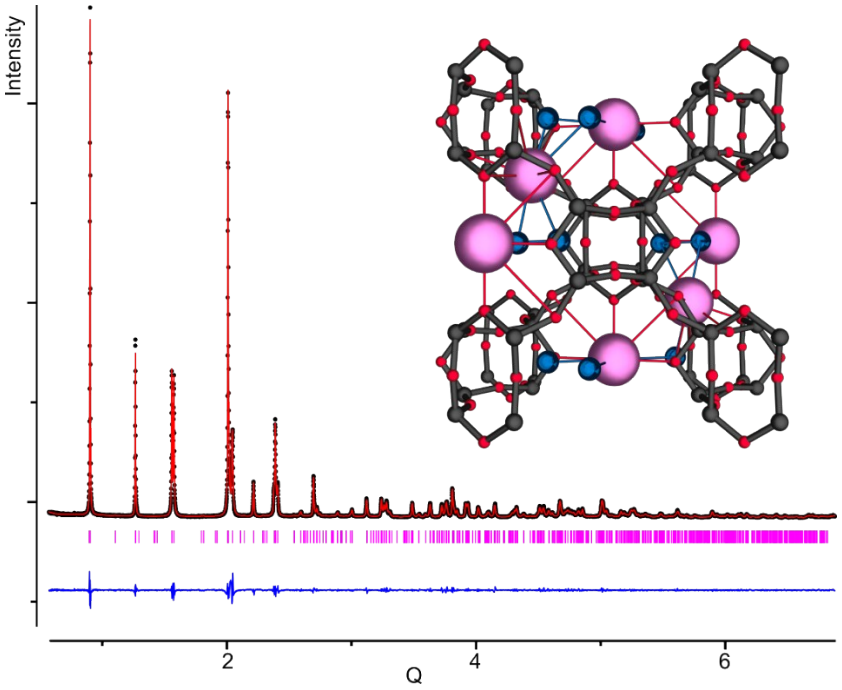

Fractional atomic coordinates and isotropic or equivalent isotropic displacement parameters ($Å^2$)

	x	*y*	*z*	U_{iso}	Occ. (<1)
O1	0.8761 (4)	−0.0017 (2)	0.0141 (3)	0.020 (2)	
O2	0.2621 (8)	0.5013 (6)	0.9192 (2)	0.021 (4)	
O3	0.5892 (2)	0.6492 (2)	0.2569 (6)	0.018 (3)	
O4	0.5892 (2)	0.3500 (2)	0.2584 (6)	0.021 (5)	
O5	−0.0006 (2)	0.2461 (8)	−0.0008 (9)	0.023 (2)	
O6	0.4989 (2)	0.3818 (3)	0.0012 (8)	0.015 (2)	
O7	0.2733 (8)	0.2297 (7)	0.9482 (6)	0.022 (3)	
O8	0.7233 (7)	0.2272 (6)	0.0520 (6)	0.015 (5)	
T1	0.1373 (5)	0.1356 (7)	0.5981 (9)	0.016 (3)	
T2	0.6215 (3)	0.3431 (4)	0.4229 (8)	0.012 (7)	
Al3	0.1226 (2)	0.8448 (4)	0.9229 (8)	0.007 (5)	
T4	0.6387 (5)	0.6341 (9)	0.0971 (9)	0.008 (6)	
ow	0.7785 (3)	0.0090 (8)	0.6552 (4)	0.024 (5)	0.982 (4)
K1	0.0	0.5	0.0	0.02 (2)	
K2	0.3426 (9)	0.7296 (8)	0.2171 (5)	0.03 (1)	0.491 (4)
ow2	0.6004 (5)	0.9983 (4)	0.7807 (2)	0.02 (5)	1.012 (2)

Crystal data
Monoclinic, $P2_1/n$
a = 9.6692 (4) Å
b = 9.8778 (3) Å
c = 9.8596 (4) Å
β = 90.001 (6)°
V = 941.69 (10) Å^3

Data collection
$2\theta_{min}$ = 7.00°, $2\theta_{max}$ = 127.50°,
$2\theta_{step}$ = 0.01°
Wavelength, 1.5175 Å

Refinement
Least-squares matrix: full, 70 Parameters
R_p = 0.07
R_{wp} = 0.078
R_{exp} = 0.039
$R(F^2)$ = 0.0905
12051 data points
$(\Delta/\sigma)_{max}$ = 1.25

Table S9 Refined XRD-pattern and parameters of dehydrated K-GIS-3.0

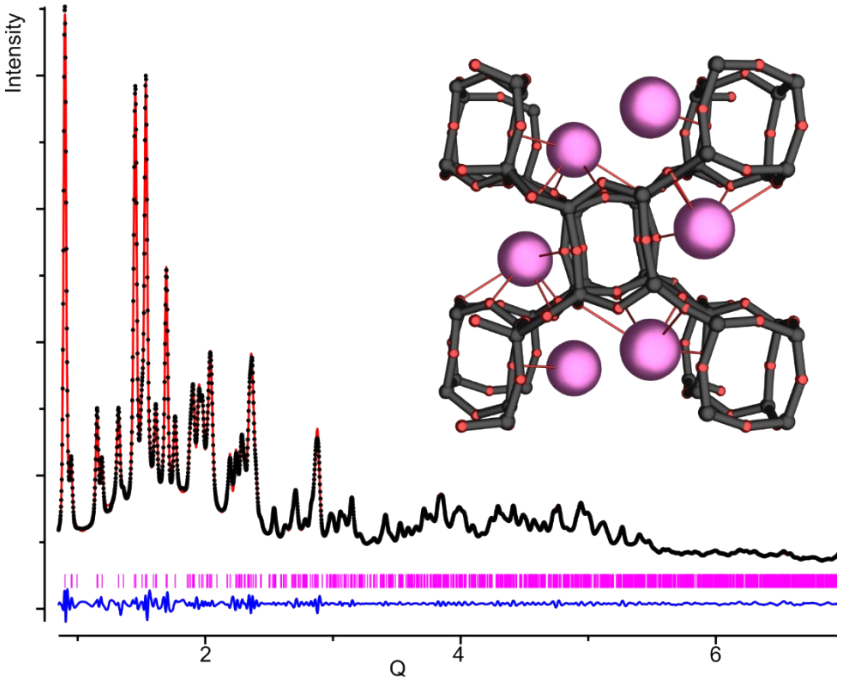

Fractional atomic coordinates and isotropic or equivalent isotropic displacement parameters (Å²)

	x	*y*	*z*	U_{iso}	Occ. (<1)
Al3	0.5615 (3)	0.6980 (4)	0.3699 (5)	0.069 (2)	
O1	0.7538 (7)	0.7421 (4)	0.3792 (5)	0.037 (4)	
O2	0.7477 (7)	0.3167 (8)	0.3173 (4)	0.037 (6)	
O3	0.5372 (4)	0.5284 (5)	0.3206 (5)	0.027 (6)	
O4	0.9527 (4)	0.5212 (4)	0.3785 (7)	0.032 (3)	
O5	0.4594 (6)	0.8111 (6)	0.2763 (6)	0.021 (5)	
O6	1.0394 (2)	0.7730 (8)	0.2771 (6)	0.038 (6)	
O7	0.9894 (6)	0.2560 (2)	0.4724 (6)	0.033 (3)	
O8	0.5036 (4)	0.2941 (5)	0.4769 (5)	0.022 (2)	
Si1	0.9326 (4)	0.3511 (5)	0.3487 (4)	0.017 (2)	
Si2	0.9382 (6)	0.6944 (3)	0.3900 (4)	0.018 (2)	
Si4	0.5604 (3)	0.3554 (4)	0.3361 (8)	0.011 (3)	
K1	0.753 (2)	0.932 (1)	0.6496 (9)	0.027 (5)	0.97 (8)

Crystal data
Monoclinic, $P2_1/n$
a = 8.570 (5) Å
b = 9.461 (5) Å
c = 10.517 (6) Å
β = 90.207 (6)°
V = 852.7 (14) Å³

Data collection
$2\theta_{min}$ = 4.976°, $2\theta_{max}$ = 59.899°,
$2\theta_{step}$ = 0.017°
Wavelength, 0.9 Å

Refinement
Least-squares matrix: full, 90 Parameters
R_p = 0.055
R_{wp} = 0.091
R_{exp} = 0.032
$R(F^2)$ = 0.1060
3320 data points
$(\Delta/\sigma)_{max}$ = 1.72

Table S10 Refined XRD-pattern and parameters of CO_2-loaded K-GIS-3.0

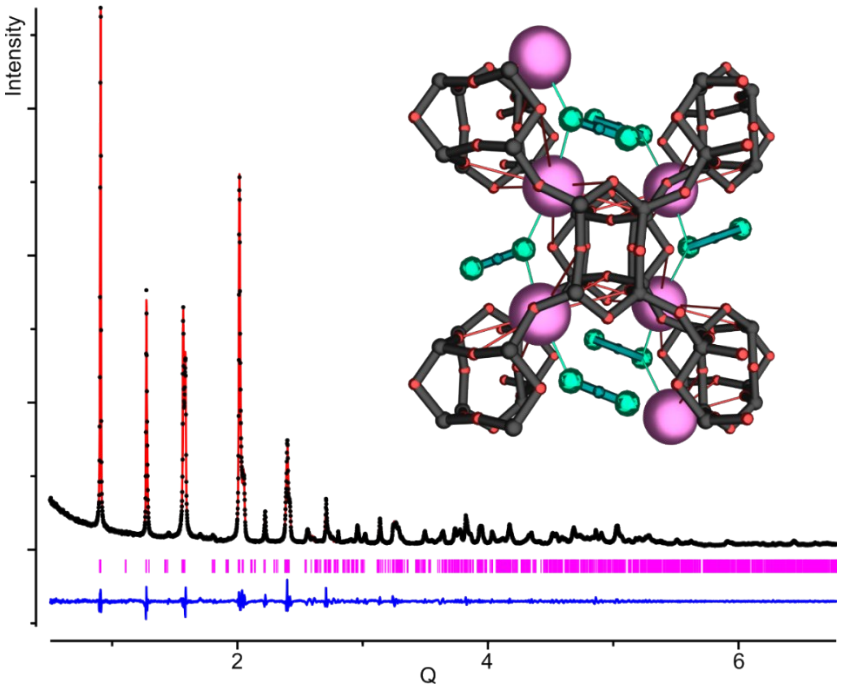

Fractional atomic coordinates and isotropic or equivalent isotropic displacement parameters ($Å^2$)

	x	*y*	*z*	U_{iso}	Occ. (<1)
O1	0.7564 (8)	0.0041 (9)	0.0809 (4)	0.010 (3)	
O2	0.3900 (4)	0.4958 (4)	0.9803 (5)	0.007 (4)	
O3	0.5812 (7)	0.6613 (7)	0.2391 (4)	0.013 (6)	
O4	0.6047 (7)	0.3488 (7)	0.2419 (4)	0.012 (7)	
O5	0.0084 (4)	0.1171 (4)	0.9930 (3)	0.017 (3)	
O6	0.5091 (5)	0.2515 (7)	0.0060 (3)	0.009 (6)	
O7	0.2390 (9)	0.2662 (9)	0.9507 (5)	0.018 (8)	
O8	0.7800 (9)	0.2878 (9)	0.0427 (6)	0.013 (3)	
Si1	0.1268 (7)	0.1524 (5)	0.5771 (7)	0.009 (2)	
Si2	0.6486 (5)	0.3673 (6)	0.4018 (7)	0.008 (4)	
Al3	0.1344 (5)	0.8581 (6)	0.9056 (7)	0.012 (2)	
Si4	0.6109 (7)	0.6623 (4)	0.0754 (7)	0.009 (9)	
K	0.276 (4)	0.254 (1)	0.263 (3)	0.015 (3)	
CO1	−0.042 (3)	0.458 (3)	0.635 (2)	0.022 (5)	
OC1	−0.151 (7)	0.497 (6)	0.661 (4)	0.045 (10)	
OC2	0.067 (7)	0.419 (6)	0.610 (4)	0.045 (10)	

Crystal data
Monoclinic, $P2_1/n$
a = 9.7097 (3) Å
b = 9.8590 (3) Å
c = 9.8932 (2) Å
β = 90.399 (4)°
V = 947.03 (5) Å^3

Data collection
$2\theta_{min}$ = 4.966°, $2\theta_{max}$ = 125.466°,
$2\theta_{step}$ = 0.02°
Wavelength, 1.5177 Å

Refinement
Least-squares matrix: full, 148 Parameters
R_p = 0.047
R_{wp} = 0.064
R_{exp} = 0.032
$R(F^2)$ = 0.12884
6026 data points
$(\Delta/\sigma)_{max}$ = 1.72

Table S11 Refined XRD-pattern and parameters of hydrated Rb-GIS-3.0

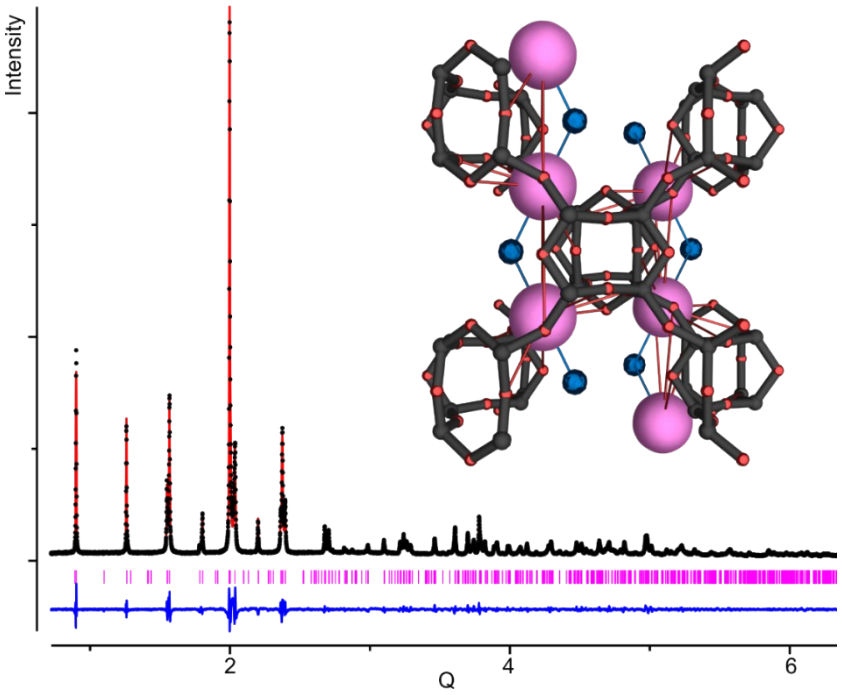

Fractional atomic coordinates and isotropic or equivalent isotropic displacement parameters ($Å^2$)

	x	*y*	*z*	U_{iso}	Occ. (<1)
O1	0.871 (11)	−0.002 (12)	0.020 (11)	0.01482	
O2	0.270 (7)	0.50 (2)	0.919 (11)	0.00462	
O3	0.586 (18)	0.650 (17)	0.256 (5)	0.01356	
O4	0.586 (18)	0.349 (17)	0.258 (5)	0.03358	
O5	0.00 (3)	0.241 (7)	−0.001 (7)	0.01774	
O6	0.499 (11)	0.373 (10)	0.001 (7)	0.02459	
O7	0.27 (3)	0.23 (2)	0.943 (14)	0.02181	
O8	0.73 (3)	0.23 (2)	0.057 (14)	0.00539	
T1	0.135 (14)	0.138 (16)	0.599 (7)	0.01307	
T2	0.621 (18)	0.344 (12)	0.420 (7)	0.01913	
Al	0.122 (19)	0.846 (12)	0.920 (7)	0.01027	
T3	0.637 (14)	0.636 (16)	0.098 (7)	0.00476	
Rb1	0.5	0.0	0.5	0.01644	0.4295
ow1	0.125	0.5	0.25	0.02824	
rb2	0.5	0.0	0.0	0.01524	0.4295
rb3	0.75	0.75	0.75	0.01957	0.5705
ow2	−0.125	0.5	0.75	0.015	

Crystal data
Monoclinic, $P2_1/n$
a = 9.7445 (8) Å
b = 9.9703 (8) Å
c = 9.9551 (8) Å
β = 90.009 (2)°
V = 967.2(2) Å^3

Data collection
$2\theta_{min}$ = 6.991°, $2\theta_{max}$ = 127.491°,
$2\theta_{step}$ = 0.01°
Wavelength, 1.5175 Å

Refinement
Least-squares matrix: full, 71 Parameters
R_p = 0.059
R_{wp} = 0.079
R_{exp} = 0.010
$R(F^2)$ = 0.1272
12051 data points
$(\Delta/\sigma)_{max}$ = 1.68

Table S12 Refined XRD-pattern and parameters of dehydrated Rb-GIS-3.0

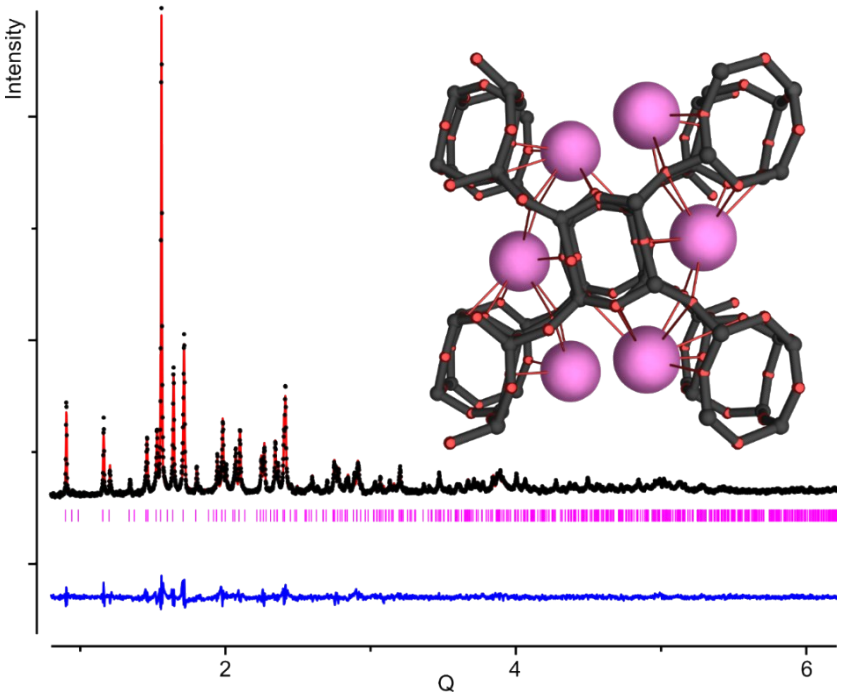

Fractional atomic coordinates and isotropic or equivalent isotropic displacement parameters (Å²)

	x	*y*	*z*	U_{iso}	Occ. (<1)
Al3	0.9381 (5)	0.1872 (5)	0.1110 (4)	0.014 (5)	
Si1	0.5580 (6)	0.8733 (5)	0.1629 (4)	0.017 (5)	
Si2	0.5669 (4)	0.1875 (3)	0.0964 (4)	0.008 (4)	
Si4	0.9362 (5)	0.8671 (5)	0.1562 (2)	0.006 (7)	
O1	0.7523 (3)	0.1910 (2)	0.0776 (5)	0.015 (3)	
O2	0.7617 (6)	0.8652 (2)	0.1739 (5)	0.020 (6)	
O3	0.9959 (7)	0.0298 (6)	0.1653 (3)	0.012 (7)	
O4	0.5013 (6)	0.0377 (6)	0.1269 (7)	0.012 (4)	
O5	0.0131 (7)	0.3001 (7)	0.2053 (5)	0.023 (2)	
O6	0.5015 (6)	0.3042 (5)	0.2048 (4)	0.016 (5)	
O7	0.5307 (6)	0.7902 (5)	0.0282 (5)	0.014 (8)	
O8	0.0030 (5)	0.7558 (4)	0.0463 (4)	0.009 (9)	
Rb	0.2504 (3)	0.0532 (5)	0.3539 (5)	0.038 (3)	0.921 (6)

Crystal data
Monoclinic, $P2_1/n$
a = 8.6476 (3) Å
b = 9.3960 (3) Å
c = 10.4845 (3) Å
β = 89.994 (12)°
V = 851.90 (3) Å³

Data collection
$2\theta_{min}$ = 2.042°, $2\theta_{max}$ = 45.042°,
$2\theta_{step}$ = 0.01°
Wavelength, 0.6927 Å

Refinement
Least-squares matrix: full, 66 Parameters
R_p = 0.038
R_{wp} = 0.056
R_{exp} = 0.003
$R(F^2)$ = 0.10629
4301 data points
$(\Delta/\sigma)_{max}$ = 1.86

Table S13 Refined XRD-pattern and parameters of CO_2-loaded Rb-GIS-3.0

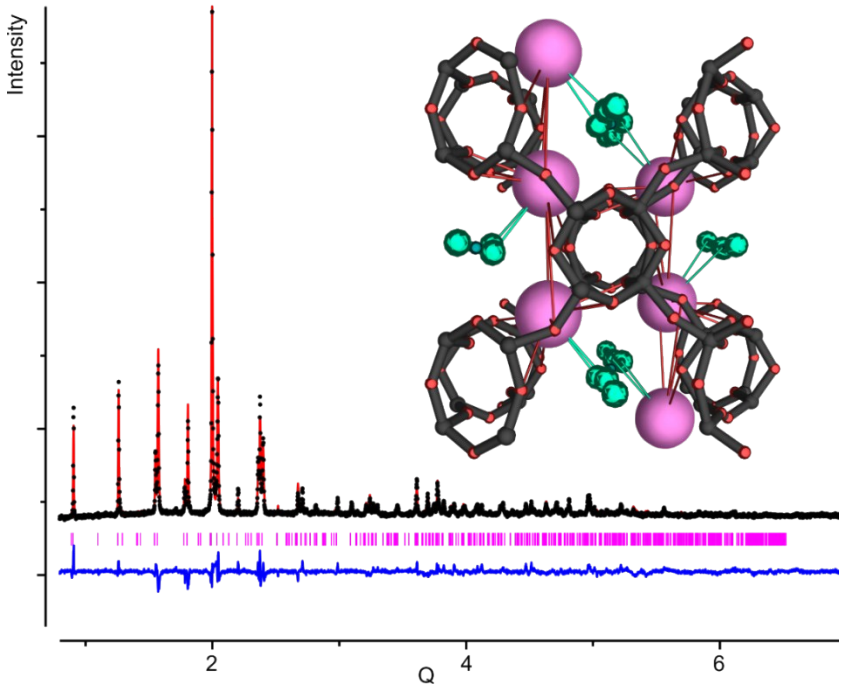

Fractional atomic coordinates and isotropic or equivalent isotropic displacement parameters ($Å^2$)

	x	*y*	*z*	U_{iso}	Occ. (<1)
Rb1	0.751 (6)	0.2564 (3)	0.2451 (3)	0.030 (7)	0.990 (5)
Si1	0.4031 (4)	0.1468 (5)	0.1082 (3)	0.010 (3)	
Al2	0.4176 (3)	0.3426 (2)	0.3686 (5)	0.009 (7)	
Si3	0.1038 (4)	0.3728 (3)	0.3741 (4)	0.012 (2)	
Si4	0.0875 (3)	0.1584 (4)	0.1220 (7)	0.013 (9)	
O1	0.2612 (3)	0.3642 (4)	0.4348 (4)	0.025 (5)	
O2	0.2425 (7)	0.1327 (4)	0.0598 (2)	0.032 (6)	
O3	0.0751 (6)	0.2427 (5)	0.2623 (5)	0.026 (5)	
O4	0.4224 (5)	0.2876 (3)	0.2041 (3)	0.019 (1)	
O5	0.0768 (9)	0.5086 (3)	0.2962 (4)	0.021 (9)	
O6	0.5022 (6)	0.2656 (3)	0.4948 (5)	0.024 (4)	
O7	0.5110 (4)	0.1958 (2)	0.9933 (4)	0.040 (6)	
O8	0.0454 (2)	0.0053 (5)	0.1722 (2)	0.038 (7)	
C1	0.5	0.0	0.5	0.031 (5)	0.983 (4)
Oc1	0.6026 (8)	0.0188 (4)	0.4482 (5)	0.062 (10)	0.983 (4)
C2	0.5	0.5	0.0	0.057 (4)	0.968 (5)
Oc2	0.6148 (10)	0.493 (2)	0.0151 (9)	0.114 (8)	0.968 (5)

Crystal data
Monoclinic, $P2_1/n$
a = 10.0083(2) Å
b = 10.02463 (11) Å
c = 9.7416 (2) Å
β = 89.997 (12)°
V = 977.36 (3) Å^3

Data collection
$2\theta_{min}$ = 2.022°, $2\theta_{max}$ = 45.022°,
$2\theta_{step}$ = 0.01°
Wavelength, 0.6927 Å

Refinement
Least-squares matrix: full, 68 Parameters
R_p = 0.032
R_{wp} = 0.052
R_{exp} = 0.023
$R(F^2)$ = 0.1057
4301 data points
$(\Delta/\sigma)_{max}$ = 1.62

Section S3: Gas adsorption studies

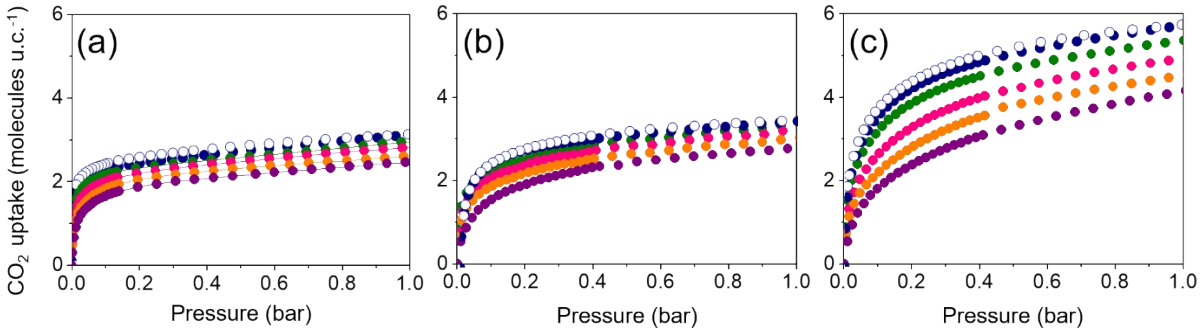

Fig. S15 CO_2 adsorption isotherms at 25 (navy), 35 (green), 50 (pink), 60 (orange), and 75 (purple) °C on (a) Na-GIS-4.7, (b) Na-A, and (c) Na-X as a function of CO_2 molecules per unit cell. Adsorption, filled symbols; desorption, open symbols.

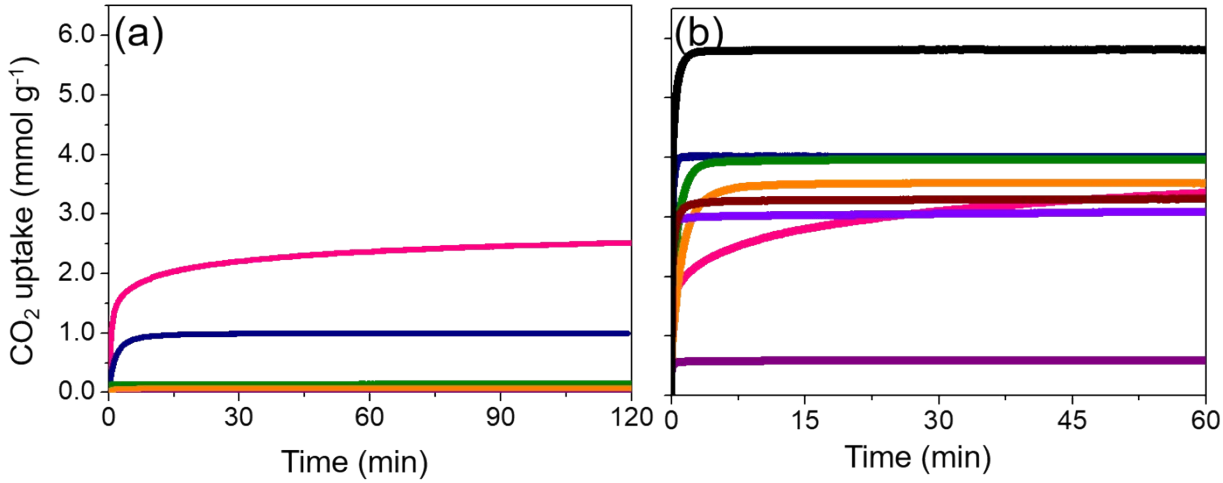

Fig. S16 CO_2 adsorption kinetics at 25 °C and (a) 0.05 bar on Li-GIS-3.0 (pink), Na-GIS-3.0 (navy), K-GIS-3.0 (green), Rb-GIS-3.0 (orange), and Cs-GIS-3.0 (purple) and (b) 1.0 bar on Li-GIS-3.0 (pink), Na-GIS-3.0 (navy), K-GIS-3.0 (green), Rb-GIS-3.0 (orange), Cs-GIS-3.0 (purple), Na-GIS-4.7 (violet), Na-A (wine), and Na-X (black).

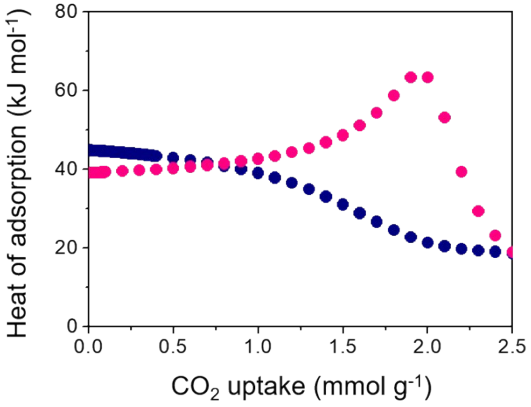

Fig. S17 Isosteric heats of CO_2 adsorption on Li-GIS-3.0 (navy) and Na-GIS-4.7 (pink) calculated using the Clausius-Clapeyron relation.

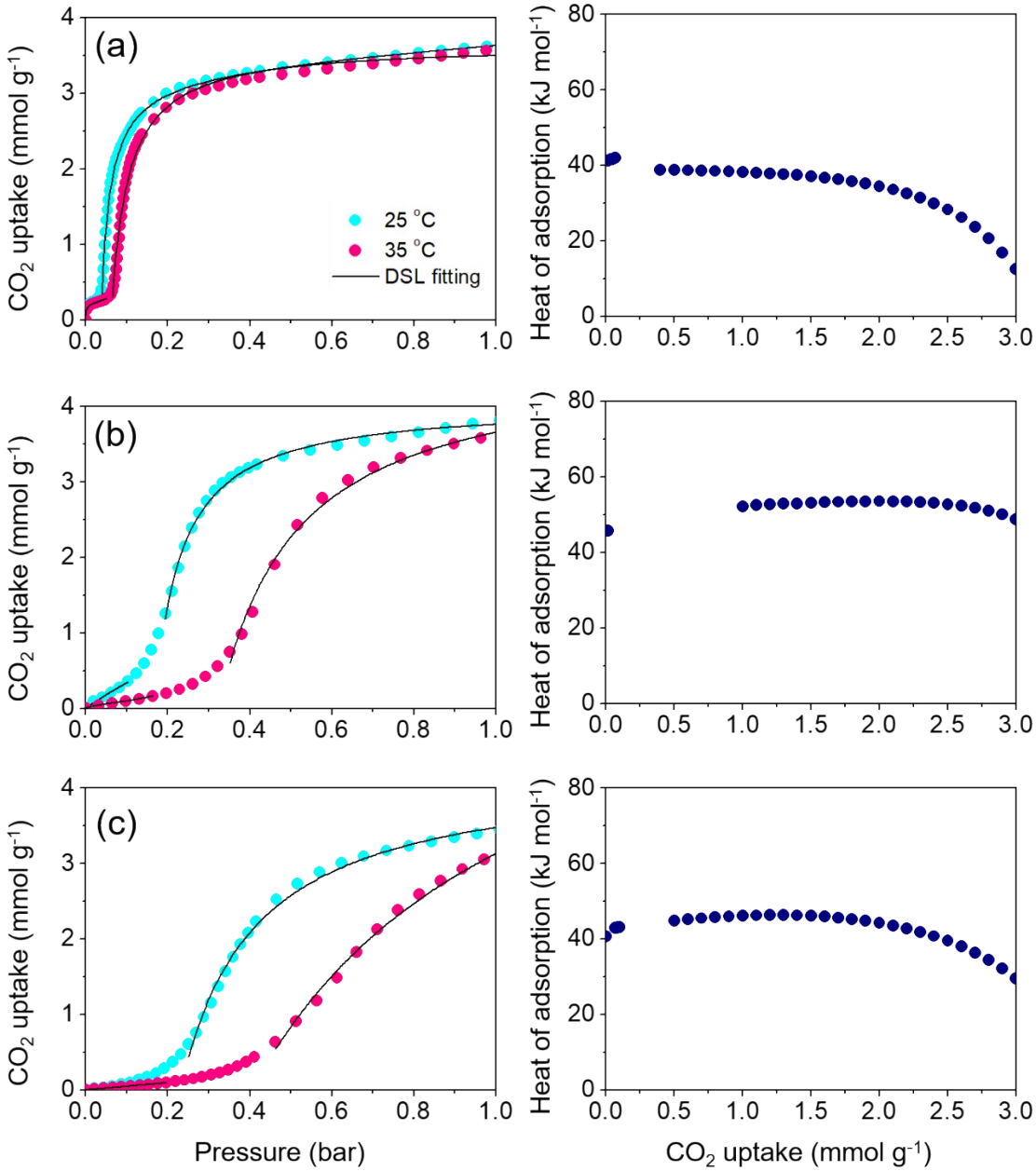

Fig. S18 CO_2 adsorption isotherms with DSL fits at 25 and 35 °C (left). Isosteric heats of CO_2 adsorption on Na-GIS-3.0 (a), K-GIS-3.0 (b) and Rb-GIS-3.0 (c) calculated using the Clausius-Clapeyron relation (right). Isosteric heat of adsorption calculations were complicated by the presence of a prominent step at low pressures in the isotherms. Generally, continuous mathematical functions were used to model experimental isotherms, which then became the input parameters for the Clausius−Clapeyron relation. Since we were not able to mathematically model the CO_2 isotherms of Na-, K- and Rb-GIS-3.0 zeolites with continuous equations over the whole pressure range, each isotherm was modelled with two Dual Site Langmuir equations. Data sets corresponding to the adsorption ranges before and after the steps were compiled and then modelled individually.

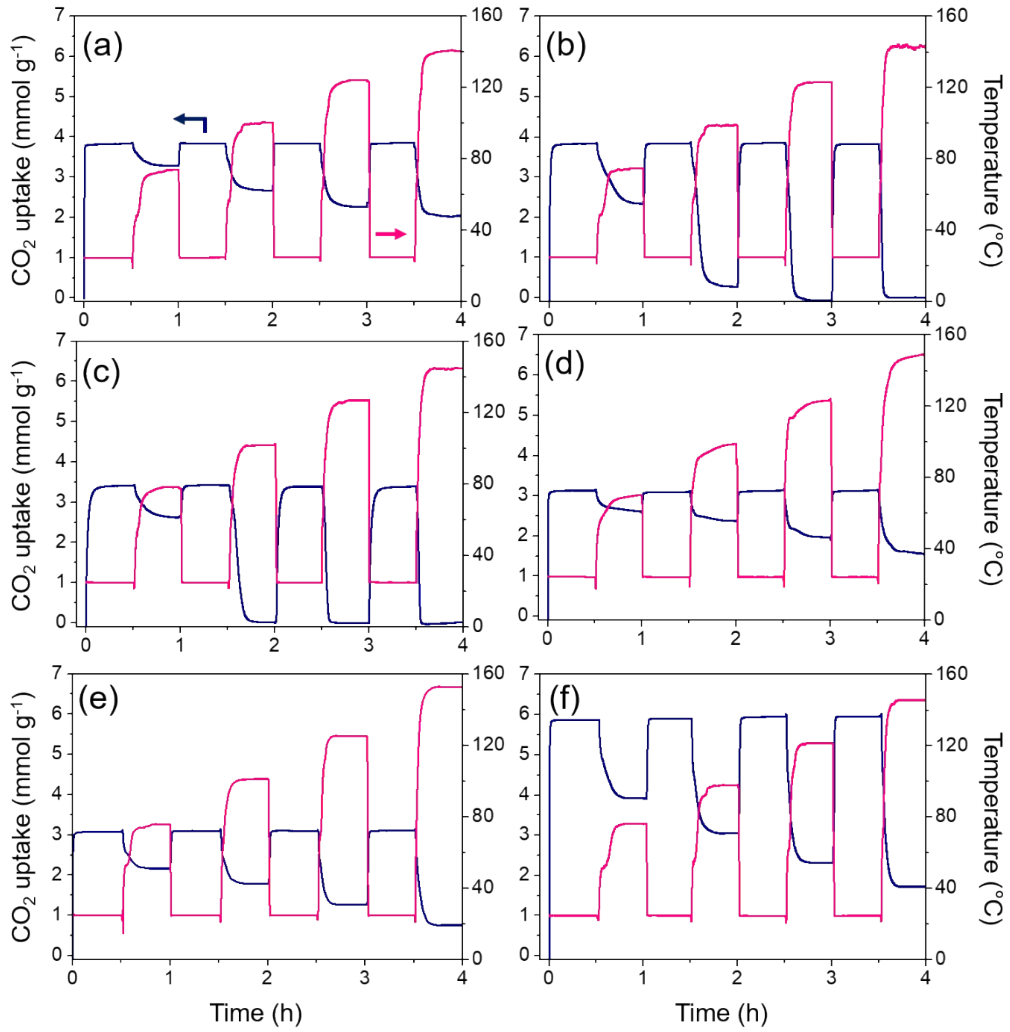

Figure S19 CO_2 adsorption-desorption profiles for (a) Na-GIS-3.0, (b) K-GIS-3.0, (c) Rb-GIS-3.0, (d) Na-GIS-4.7, (e) Na-A, and (f) Na-X. Each profile was measured in the TSA cycle at 1.0 bar under different temperatures.

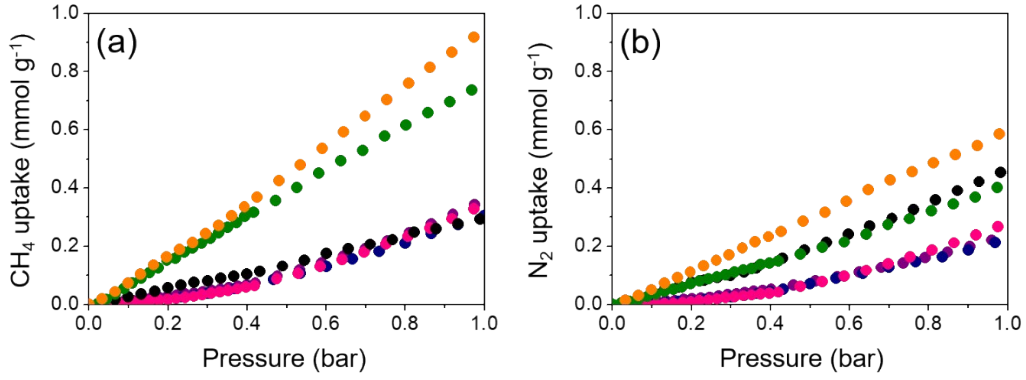

Fig. S20 (a) CH_4 and (b) N_2 adsorption isotherms at 25 °C on Na-GIS-3.0 (purple), K-GIS-3.0 (navy), Rb-GIS-3.0 (pink), Na-GIS-4.7 (black), Na-A (green) and Na-X (orange).

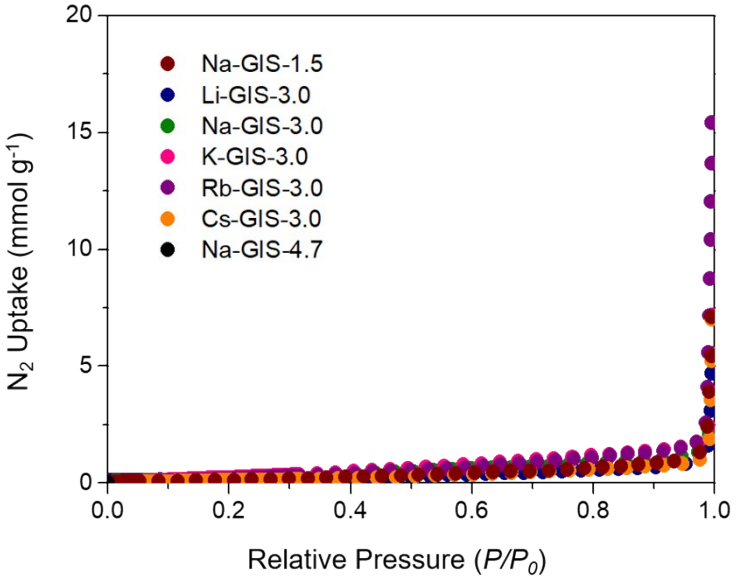

Fig. S21 N_2 adsorption isotherms on various alkali cation forms of GIS zeolites with different Si/Al ratios at -196 °C.

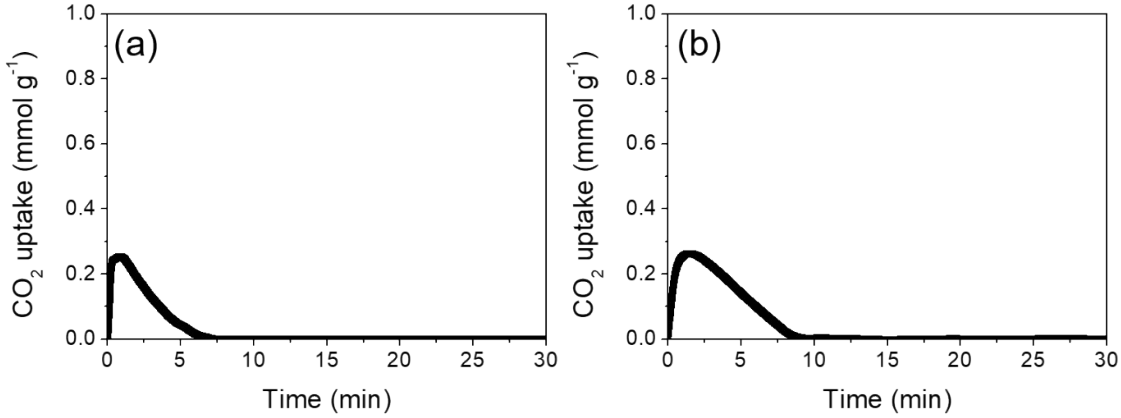

Fig. S22 CO_2 adsorption profiles at 25 °C of (a) K-GIS-3.0 and (b) Rb-GIS-3.0 obtained in a wet gas mixture consisting of 50% CO_2, 47% CH_4, and 3% H_2O.

Table S14 CO_2/N_2 (0.5 bar CO_2 and 0.5 bar N_2) and CO_2/CH_4 (0.5 bar CO_2 and 0.5 bar CH_4) selectivities of zeolites with different topologies and compositions at 25 °C[a]

Material	CO_2/N_2 selectivity	CO_2/CH_4 selectivity
Na-GIS-3.0	44	32
K-GIS-3.0	48	36
Rb-GIS-3.0	38	28
Na-GIS-4.7	14	16
Na-A	17	8
Na-X	17	11

[a] The selectivity is defined as $(q_1/q_2)(p_1/p_2)$, where q_1 and q_2 are the equilibrium molar uptakes of components 1 and 2 taken from the corresponding single component isotherms and p_1 and p_2 are the partial pressures of components 1 and 2.

Section S4 Methods and used equipments

S4.1 General Characterization

Powder X-ray diffraction (PXRD) patterns were recorded on a PANalytical X´Pert diffractometer (Cu Kα radiation) with an X´Celerator detector. Data were collected with a fixed divergence slit (0.50°) and Soller slits (incident and diffracted = 0.04 rad) (Fig. S1 and S4-S6). Crystal morphology and average size were determined using a JEOL JSM-6510 SEM (Fig. S1 and S6). Elemental analysis was performed by the Analytical Laboratory of the Pohang Institute of Metal Industry Advancement. The analysis for Si, Al, Li, Na, K, Rb, and Cs was carried out by using a Jarrell-Ash Polyscan 61E inductively coupled plasma spectrometer in combination with a Perkin-Elmer 5000 atomic absorption spectrophotometer (Table S2). Thermogravimetric and differential thermal analyses (TGA/DTA) were performed on an SII EXSTAR 6000 thermal analyzer at a heating rate of 10°C min^{-1}. ^{13}C solution NMR measurements for ATMEA chloride was carried out in 5 mm quartz tubes using a Bruker AVANCE III 300 spectrometer (Fig. S2). The ^{13}C NMR spectrum was recorded at a ^{13}C frequency of 75.475 MHz with a π/2 rad pulse length of 10.2 ms and a recycle delay of 1.5 s. Solid-state multinuclear NMR measurements were performed using a Bruker AVANCE II 500 spectrometer at a spinning rate of 21 kHz. The ^{13}C MAS NMR spectrum was recorded at a ^{13}C frequency of 125.758 MHz with a π/2 rad pulse length of 4.8 μs, a recycle delay of 5.0 s, and an acquisition of ca. 1800 pulse transients (Fig. S2). The ^{29}Si MAS spectra were recorded at a ^{29}Si frequency of 99.357 MHz with a π/2 rad pulse length of 4.0 μs, recycle delay of 20 s, and an acquisition of ca. 1000 pulse transients (Fig. S3). The ^{13}C and ^{29}Si shifts are referend relative to tetramethylsilane (TMS). The ^{27}Al MAS NMR spectra were recorded at a ^{27}Al frequency of 130.318 MHz with a π/2 rad pulse length of 1.0 μs, a recycle delay of 1.0 s, and an acquisition of ca. 700 pulse transients (Fig. S3). The ^{27}Al chemical shifts are referenced relative to an $Al(H_2O)_6^{3+}$ solution.

S4.2 PXRD measurements

High-resolution PXRD patterns were collected at station 9B and 2D at the Pohang Acceleration Laboratory (PAL), Pohang, Korea (Fig. 2 and Fig. S14 and Tables S4-S13). At station 9B, the PXRD patterns of hydrated samples were measured at room temperature in flat plate mode with spin rotation using monochromated X-rays (λ = 1.51750 Å). The detector arm of the vertical scan diffractometer consists of seven sets of Soller slits, flat Ge(111) crystal analyzers, anti-scatter baffles, and scintillation detectors, with each set separated by 20º. Data were collected at room temperature with a step size of 0.01º and overlaps of 2º to the next detector bank over the 2θ range 7.0 – 147.5º. The patterns of dehydrated samples were obtained under the same conditions as those described above, after heating from room temperature to 250 °C at a ramping rate of 10 °C min^{-1} and holding at the same temperature for 3 h under a dynamic vacuum of 10^{-3} Torr. Also, after exposure of dehydrated samples to 1.0 bar of pure CO_2 at 25 ºC for 30 min in the ceramic chamber, PXRD data were obtained.

At station 2D, the PXRD patterns of dehydrated and CO_2 adsorbed samples were collected in capillary mode. Prior to measurements, each zeolite sample was packed into a 0.7 mm quartz capillary and evacuated under a vacuum of 10^{-3} Torr at 250 °C for 3 h. Then, CO_2 gas (99.999%, Linde) was introduced to the samples as a function of pressure, and the pressure was kept constant for 30 min. Data were collected at room temperature using an MX225-HS CCD area detector with monochromated X-rays (λ = 0.6927 and 0.9000 Å). The sample-to-detector distance, omega scan range, and exposure time were fixed at 66 mm, 360° and 60s, respectively.

S4.3 PXRD analysis.

PXRD patterns were indexed using the DICVOL,[S9] TREOR,[S10] and McMaille[S11] algorithms, as well as with FOX,[S1] which also served to assign crystallographic directions. Starting models for Rietveld refinement were obtained combining framework optimization by GULP[S2,S3] (using the Catlow library[S4,S5]) with guest molecule and cation search by FOX. Rietveld refinement was done using GSAS[S7,S8].

S4.4 Solid-state NMR measurements

^{27}Al and ^{23}Na solid-state NMR experiments were conducted on a Bruker Avance III 500 NMR spectrometer (11.7 T) equipped with a 4-mm H/X/Y MAS probe (Fig. S8, S9, S12 and S13), which operates at Larmor frequencies of 500.87, 130.52, and 132.49 MHz for ^{1}H, ^{27}Al, and ^{23}Na, respectively. The samples were spun up to 15 kHz MAS frequency. Typically, 1024 scans (recycle delay of 2 s) were recorded for ^{27}Al MAS NMR, and 1024 scans (recycle delay of 2 s) were recorded for ^{23}Na MAS NMR, with ^{1}H decoupling using SW_f-SPINAL method. The RF strengths used for ^{27}Al, ^{23}Na, and ^{1}H for decoupling are 125, 125, and 83 kHz, respectively. ^{27}Al and ^{23}Na NMR were recorded with 15° pulse. ^{27}Al triple-quantum (3Q) MAS NMR experiments were performed using standard three-pulse *z*-filtered pulse program (Fig. S6). 600 slices were collected with 72 numbers of transients at a t_1 increment of 10 μs for ^{27}Al 3Q-MAS NMR, respectively. ^{29}Si MAS NMR experiments were conducted on a Bruker Avance III 300 NMR spectrometer (7.1 T) which operates at Larmor frequencies of 300.13 MHz for ^{1}H and 59.62 MHz for ^{29}Si (Fig. 2 and Fig. S7, S10 and S11). The samples were spun at 10 kHz with ^{1}H decoupling using SW_f-SPINAL sequences. The RF strengths used for ^{29}Si and ^{1}H for decoupling are 66 and 55 kHz respectively. Typically, 720 transients were collected with a recycle delay of 120 s were recorded for hydrated sample. 320 transients with a recycle delay of 600 s were recorded for dehydrated and CO_2 adsorbed samples. ^{87}Rb (Larmor frequency of 262.16 MHz) NMR measurements were measured on an Avance Neo 800 NMR spectrometer (18.8 T), equipped with a 1.9 mm H/X/Y probe, at a spinning frequency of 40 kHz (Fig. S9). 131072 transients were acquired with a recycle delay of 2 s. RF fields used were 66 kHz for ^{87}Rb and 10 kHz for ^{1}H spinal-64 decoupling. ^{1}H and ^{29}Si chemical shifts were referenced against TMS, whereas ^{27}Al, ^{23}Na, and ^{87}Rb chemical shifts were referenced against 1.0 M solutions of $Al(NO_3)_3$, NaCl, and RbCl, respectively.

S4.5 Gas adsorption experiments

The CO_2, N_2, and CH_4 adsorption isotherms were measured using a Setaram PCTPro E&E or a Mirae SI nanoPorosity-XQ analyzer (Fig. 1 and Fig. S15 and S20). Before each experiment, 0.1 g of sample was evacuated under a vacuum of 10^{-3} Torr at 250 °C for 3 h. The

increment of the reservoir pressure (ΔP) was set as 0.1 bar, and, if required, ΔP was set as 0.004 bar to discriminate pressures at step points. The equilibrium conditions were fixed at 98% of the calculated uptake or at the maximum equilibration time of 30 min for each isotherm point. Adsorption kinetics was performed on a Setaram PCTPro E&E analyzer at 25 °C and 0.05 and 1.0 bar (Fig. S16). CO_2 adsorption at 25 °C in the presence of a small amount (3%) of water was carried out on a Micromeritics Autochem II 2920 chemisorption analyzer equipped with a cold trap for H_2O removal in front of a TCD detector (Fig. S22). Before the measurements, 0.1 g of sample was degassed at 250 °C for 3 h under N_2 flow (50 cm^3 min^{-1}). CO_2 adsorption–desorption profiles in the temperature swing adsorption (TSA) cycle under static condition were carried out using a Setaram PCTPro E&E analyzer using high-purity CO_2 (Fig. S19). Prior to the experiments, 0.1 g of sample was activated under the conditions described above. The TSA cycle was measured between 25 and 75 °C. Regenerability and CO_2 working capacity of sample calculated from TSA data (Fig. 4a and Fig. S19), with adsorption at 25 °C and desorption at 100 °C using pure CO_2 at 1.0 bar. The CO_2 working capacity $^{\Delta N_{CO_2}}$ (mmol g^{-1}) and regenerability R (%), are defined as follows:

$$\Delta N_{CO_2} = N_{CO_2}^{ads} - N_{CO_2}^{des} \quad (1)$$

$$R = \left(\Delta N_{CO_2} / N_{CO_2}^{ads}\right) \times 100 \quad (2)$$

where $N_{CO_2}^{ads}$ and $N_{CO_2}^{des}$ are the CO_2 uptakes at low and high temperatures, respectively.

CO_2 adsorption–desorption profiles in the TSA cycle under dynamic conditions (Fig. 4b) were collected using a Scinco TGA N1500 thermogravimetric analyzer. Before the measurements, 0.1 g of sample was degassed at 250 °C for 3 h under N_2 flow (50 cm^3 min^{-1}). CO_2 adsorption was carried out using a dry gas mixture containing 50% CO_2 and CH_4 balance at 25 °C. After adsorption for 30 min, the gas was switched to pure CO_2 flow (50 cm^3 min^{-1}). Then, the temperature was increased from 25 to 100 °C with a ramping rate of 10 °C min^{-1} and maintained at 100 °C for 30 min. The adsorption–desorption cycle was repeated 10 times.

S4.6 Calculation of isosteric heat of CO_2 adsorption

The experimental adsorption isotherms obtained were fitted using the dual-site Langmuir (DSL) equation. The fitting details can be found in our recent report,[S12] and all fitted DSL parameters are given in Tables S15 and S16.

The heats of adsorption were calculated by applying the Clausius-Clapeyron equation to the two adsorption isotherms at 25 and 35 °C (or 45 °C):

$$\left[\frac{\partial lnP}{\partial(1/T)}\right]_q = \frac{-\Delta Q}{R} \quad (3)$$

where ΔQ is the heat of adsorption, P pressure, R the gas constant, and T temperature.

Table S15 Dual-site Langmuir parameters for CO_2 adsorption on Li-GIS-3.0 and Na-GIS-4.7

Li-GIS-3.0	25 °C	35 °C	50 °C	60 °C	75 °C
$m^{(b)}$ (mol kg^{-1})	1.7902	1.9211	1.5589	1.6103	1.4140
b (bar^{-1})	83.9659	43.3226	54.6397	26.1338	25.6122
$m^{(d)}$ (mol kg^{-1})	2.3931	2.6011	2.8723	2.7396	2.2043
d (bar^{-1})	1.5252	0.8885	1.0102	0.8993	1.3862
R^2	0.9999	0.9997	0.9998	0.9998	0.9999
Na-GIS-4.7	25 °C	35 °C	50 °C	60 °C	75 °C
$m^{(b)}$ (mol kg^{-1})	1.6010	1.9729	1.8051	1.3533	1.5430
b (bar^{-1})	1.3085	401.9046	259.0399	2.4392	1.2088
$m^{(d)}$ (mol kg^{-1})	2.0784	1.7097	1.5445	1.6317	1.6255
d (bar^{-1})	637.0624	1.2731	1.8087	164.3820	101.1751
R^2	0.9972	0.9971	0.9984	0.9987	0.9993

Table S16 Dual-site Langmuir parameters for CO_2 adsorption on Na-, K- and Rb-GIS-3.0

	Pre-step*		Post-step†	
Na-GIS-3.0	25 °C	35 °C	25 °C	35 °C
$m^{(b)}$ (mol kg^{-1})	1.0127	0.1938	3.2844	1.5602
b (bar^{-1})	3.0268	723.1870	45.7286	24.8367
$m^{(d)}$ (mol kg^{-1})	0.1980	1.3995	3.8835	2.0859
d (bar^{-1})	1214.7231	1.3297	0.1249	24.8376
P_{step} (bar)	-	-	-0.0370	-0.0616
R^2	0.9998	0.9997	0.9992	0.9942
K-GIS-3.0	25 °C	35 °C	25 °C	35 °C
$m^{(b)}$ (mol kg^{-1})	2.3268	-0.2684	1.6425	2.0515
b (bar^{-1})	1.0604	-1.9489	15.9961	5.4216
$m^{(d)}$ (mol kg^{-1})	0.7592	0.0415	2.4080	2.6086
d (bar^{-1})	1.8052	58.7463	15.9954	5.4216
P_{step} (bar)	-	-	-0.1687	-0.3244
R^2	0.9958	1.0000	0.9979	0.9967
Rb-GIS-3.0	25 °C	35 °C	25 °C	35 °C
$m^{(b)}$ (mol kg^{-1})	1.1497	1.8934	1.8884	3.1758
b (bar^{-1})	0.4516	0.1308	5.6092	1.5006
$m^{(d)}$ (mol kg^{-1})	0.8379	1.8834	2.3969	3.4595
d (bar^{-1})	0.3660	0.1260	5.6092	1.5007
P_{step} (bar)	-	-	-0.2309	-0.4037
R^2	0.9928	0.9970	0.9977	0.9973

*The fitting parameters for the pre-step adsorption. †The fitting parameters for the post-step adsorption.

References

S1 V. Favre-Nicolin and R. Černý, *J. Appl. Crystallogr.* 2002, **35**, 734.

S2 J. D. Gale, *Z. Kristallogr.* 2005, **220**, 552.

S3 J. D. Gale, *J. Chem. Soc. Faraday Trans.* 1997, **93**, 629.

S4 K.-P. Schröder, J. Sauer, M. Leslie, C. Richard, A. Catlow and J. M. Thomas, *Chem. Phys. Lett.* 1992, **188**, 320.

S5 J. D. Gale and N. J. Henson, *J. Chem. Soc. Faraday Trans.* 1994, **90**, 3175.

S6 G. Maurin, P. L. Llewellyn and R. G. Bell, *J. Phys. Chem. B* 2005, **109**, 16084.

S7 A. C. Larson and R. B. Von Dreele, *General Structure Analysis System (GSAS), Los Alamos National Laboratory Report LAUR 86-748*, Los Alamos National Laboratory: Los Alamos, NM, 2004.

S8 B. H. Toby, *J. Appl. Crystallogr.* 2001, **34**, 210.

S9 A. Boultif and D. Louër, *J. Appl. Crystallogr.* 1991, **24**, 987.

S10 P.-E. Werner, L. Eriksson and M. Westdahl, *J. Appl. Crystallogr.* 1985, **18**, 367.

S11 A. Le Bail, *Powder Diffraction* 2004, **19**, 249.

S12 J. G. Min, K. C. Kemp, H. Lee and S. B. Hong, *J. Phys. Chem. C* 2018, **122**, 28815.